

See discussions, stats, and author profiles for this publication at: <https://www.researchgate.net/publication/265299731>

# Investigating the Intrinsic Aggregation Potential of Evolutionarily Conserved Segments in p53

ARTICLE *in* BIOCHEMISTRY · SEPTEMBER 2014

Impact Factor: 3.02 · DOI: 10.1021/bi500825d · Source: PubMed

---

CITATIONS

2

---

READS

73

## 8 AUTHORS, INCLUDING:



Dhiman Ghosh

Indian Institute of Technology Bombay

13 PUBLICATIONS 93 CITATIONS

[SEE PROFILE](#)



Srivastav Ranganathan

Indian Institute of Technology Bombay

6 PUBLICATIONS 26 CITATIONS

[SEE PROFILE](#)



Anoop Arunagiri

University of Michigan

12 PUBLICATIONS 127 CITATIONS

[SEE PROFILE](#)



Samir Maji

Indian Institute of Technology Bombay

69 PUBLICATIONS 1,838 CITATIONS

[SEE PROFILE](#)

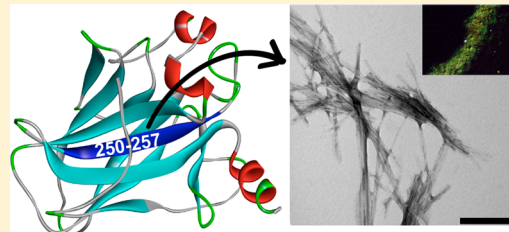
# Investigating the Intrinsic Aggregation Potential of Evolutionarily Conserved Segments in p53

Saikat Ghosh, Dhiman Ghosh, Srivastav Ranganathan, A Anoop, Santosh Kumar P, Narendra Nath Jha, Ranjith Padinhateeri, and Samir K. Maji\*

Department of Biosciences and Bioengineering, IIT Bombay, Powai, Mumbai 400076, India

## Supporting Information

**ABSTRACT:** Protein aggregation and amyloid formation are known to play a role both in diseases and in biological functions. Transcription factor p53 plays a major role in tumor suppression by maintaining genomic stability. Recent studies have suggested that amyloid formation of p53 could lead to its loss of physiological function as a tumor suppressor. Here, we investigated the intrinsic amyloidogenic nature of wild-type p53 using sequence analysis. We used bioinformatics and aggregation prediction algorithms to establish the evolutionarily conserved nature of aggregation-prone sequences in wild-type p53. Further, we analyzed the amyloid forming capacity of conserved and aggregation-prone p53-derived peptides PILTIITL and YFTLQI *in vitro* using various biophysical techniques, including all atom molecular dynamics simulation. Finally, we probed the seeding ability of the PILTIITL peptide on p53 aggregation *in vitro* and in cells. Our data demonstrate the intrinsic amyloid forming ability of a sequence stretch of the p53 DNA binding domain (DBD) and its aggregation templating behavior on full-length and p53 core domain. Therefore, p53 aggregation, instigated through an amyloidogenic segment in its DBD, could be a putative driving force for p53 aggregation *in vivo*.



**A**myloidosis is a group of diseases characterized by abnormal protein folding and assembly into insoluble protein fibrils.<sup>1,2</sup> Depending upon the disease, protein fibrils are deposited either extracellularly or intracellularly.<sup>1</sup> Deposition of amyloid fibrils causes cell and organ dysfunction and eventually cell death. More than 24 different proteins and polypeptides are known to form amyloid deposits *in vivo* that are associated with human diseases.<sup>1</sup> In addition, many proteins, which are apparently not associated with any disease, have also been found to form amyloid fibrils *in vitro* under certain environmental conditions,<sup>3,4</sup> suggesting that amyloid fibril formation might be a generic property of (m)any proteins and polypeptides.<sup>5</sup> The exact structure of amyloid fibrils is very difficult to determine because of their insolubility and noncrystallinity.<sup>2</sup> However, they can be characterized as cross- $\beta$ -sheet structures, with the hydrogen bonds parallel and the  $\beta$ -strands perpendicular to the fibril axis.<sup>2</sup> Substantial efforts have been made to understand the molecular and physicochemical factors that transform a natively folded/unfolded protein into amyloid fibrils. Moreover, many studies have supported the fact that amyloid fibrils are widespread in nature for performing native biological functions of the host.<sup>6–8</sup>

Transcriptional regulator p53 plays an essential role in tumor suppression.<sup>9,10</sup> When p53 is active inside the nucleus as a tetrameric Zn-bound form, it binds to DNA and thus suppresses cell cycle progression or induces apoptosis in response to DNA damage.<sup>9,11</sup> In normal cells, p53 levels are tightly regulated as a result of a short half-life (15–30 min)<sup>12</sup> and cannot be detected by immunocytochemistry.<sup>13</sup> It has been

reported that point mutations in p53 promote oncogenesis through multiple mechanisms.<sup>14,15</sup> These include loss of wild-type p53 functions in cells, gain of “dominant-negative” functions, in which mutant p53 is incorporated into a functional tetramer of wild-type p53, making it nonfunctional, and gain of oncogenic functions like invasiveness, increased levels of migration, and unregulated cell proliferation.<sup>14</sup> In addition to point mutations, nonsense or frameshift mutations in p53 might completely abolish the expression of the protein.<sup>14</sup> Other than these mechanisms, cancer-related point mutations in any of the three domains of p53 (N-terminal, DNA binding, and tetramerization) prolong the half-life of p53, leading to its accumulation in cells, which can be readily detected by immunocytochemistry.<sup>13</sup> Interestingly, many cancers are often characterized by the loss of function of p53 that frequently accumulates in nucleus as well as in some cases in the cytoplasm.<sup>16–20</sup> The exact reason and nature of these cytoplasmic p53 inclusions are not clearly understood.

Recent findings suggest that the individual domains as well as the full-length p53 protein aggregate into amyloids *in vitro*. For example, the recombinant protein fragments, DNA binding domain (DBD),<sup>21</sup> and tetramerization domain (TD)<sup>22</sup> of p53 have been shown to form amyloid under certain experimental conditions *in vitro*. Furthermore, it was also shown that the isolated N-terminal transactivation domain (residues 1–63) of

Received: July 4, 2014

Revised: September 1, 2014

Published: September 2, 2014

p53 formed aggregates under acidic conditions, which bind to thioflavin T (ThT), suggesting that those aggregates are amyloid fibrils.<sup>23</sup> The level of aggregation of the wild-type DBD was observed to increase exponentially in the presence of zinc-depleted DBD (apo DBD), which suggested that apo DBD catalyzed the aggregation of the wild-type DBD.<sup>24</sup>

Recently, it has been demonstrated that full-length p53 can form both oligomers and amyloid fibrils *in vitro*.<sup>25,26</sup> In addition to biophysical studies, immunofluorescence colocalization studies using amyloid fibril and oligomer-specific antibodies, OC and A11, respectively, have identified intracellular amyloid aggregates of mutant p53 in tumor tissue biopsies and cancer cell lines.<sup>25–27</sup> Moreover, p53 aggregation and amyloid formation by inflammation-derived cholesterol 5,6-secoesterol aldehydes, atheronal-A (KA) and atheronal-B (ALD), have also been reported.<sup>28</sup> Recently, it has been shown that misfolded mutant p53 can cause a loss of wild-type p53 functions using a mechanism similar to that of prions.<sup>26</sup> Interestingly, it also has been reported that mutant p53 can co-aggregate with its paralogs p63 and p73 and can attenuate their antitumorigenic functions with a subsequent gain of oncogenic functions.<sup>29</sup> In another study, it was reported that p53 aggregates could enter cells and template the aggregation of endogenous p53.<sup>30</sup> Therefore, previous *in vitro* and *in vivo* studies clearly indicate that aggregation and amyloid formation of p53 in cytoplasm and/or nucleus could result in a loss of function of p53 as a tumor suppressor.<sup>25–28</sup> Understanding the mechanism of aggregation of p53 into amyloid and the segments of p53 that are potentially involved in amyloid formation is important for developing therapeutics against p53 loss of function.

In this study, we analyzed the intrinsic amyloid forming tendency of p53 using the amyloid prediction algorithm TANGO,<sup>31</sup> which showed that human p53 possesses two regions with high amyloidogenicity corresponding to the amino acid sequences PILTIITL (p53 250–257) and YFTLQI (p53 327–332). To gain further insight into the amyloid forming capabilities of p53 across species, we performed multiple-sequence alignment and TANGO analysis of p53 from 60 different species. The results suggest a conservation of the p53 DBD across species. Importantly, the putative amyloidogenic regions (PILTIITL and YFTLQI), as predicted by TANGO, also showed a high degree of conservation. We analyzed the aggregation and amyloid formation by these two sequences using synthetic peptides corresponding to PILTIITL (eight residues, P8) and YFTLQI (six residues, P6) *in vitro*, using various biophysical techniques, and our data showed amyloid formation by the P8 peptide. The aggregation of these peptides was further probed in atomistic detail using all atom MD simulations; these results suggested a high  $\beta$ -sheet forming potency of P8, while these characteristics were observed to a lesser degree in P6. Interestingly, the “amyloid gatekeeper amino acid” (arginine, Arg)<sup>32</sup> substitution of the residues involved in H-bonding, as analyzed from our *in silico* study, showed a diminished level of aggregation *in vitro*. Residue shuffling of P8 also abolished its ability to aggregate. Further, we showed P8 fibrils induced aggregation of p53 core domain *in vitro* and full-length p53 aggregation in cells. Overall, this study shows the aggregation capabilities of a conserved stretch in wild-type p53 (PILTIITL), which might drive full-length p53 aggregation *in vivo*.

## ■ EXPERIMENTAL PROCEDURES

**Chemicals and Reagents.** All chemicals used for the experimental studies were purchased from Sigma and Merck and were of high purity. Water was double distilled and deionized using a Milli-Q system (Millipore Corp., Bedford, MA). Peptides were custom synthesized by USV Ltd. using a solid-phase peptide synthesis method and purified. Peptide mass was confirmed by matrix-assisted laser desorption ionization time-of-flight (MALDI-TOF) mass spectrometry, and >98% pure peptides were used for the aggregation study.

**Prediction of Aggregation Propensity Using Prediction Algorithms.** To ascertain and predict any inherent aggregation propensity in the p53 tumor suppressor protein, p53 protein sequences from various organisms were subjected to TANGO<sup>31</sup> and WALTZ<sup>33</sup> analysis, which predicts the propensity of amyloid aggregation in proteins and peptides. The TANGO algorithm is primarily based on simple physiochemical principles of secondary structure formation and the assumption that aggregating sequence in proteins is fully buried.<sup>31</sup> TANGO was performed at pH 7.0, 298 K, and an ionic strength of 0.02. The WALTZ algorithm uses a position-specific scoring matrix to predict aggregation-prone residues in proteins.<sup>33</sup> WALTZ analysis was performed at pH 7.0 using a threshold of “best overall performance” for analyzing the 60 species and “high sensitivity” for the separate analysis of human p53. Algorithms AGGRESCAN,<sup>34–36</sup> PASTA,<sup>37</sup> and Zipper DB<sup>38</sup> were used to predict “hot spots” of  $\beta$ -aggregation in human p53.

**Multiple-Sequence Alignment (MSA) and Phylogenetic Tree Analysis.** The p53 protein sequences for various organisms were obtained from the UniProtKB protein database. Multiple-sequence alignment was performed to search for sequence similarity between the p53 sequences of various species using Clustal Omega (clustalO).<sup>39</sup> The phylogenetic tree was constructed using TreeDyn.<sup>40</sup>

**In Vitro Aggregation Studies of p53 (250–257, PILTIITL) and p53 (327–332, YFTLQI).** Peptides (P8, NH<sub>2</sub>-PILTIITL-COOH; P6, NH<sub>2</sub>-YFTLQI-COOH) were dissolved in 0.5 mL of 5% D-mannitol and 0.01% sodium azide (pH 5.5) at a concentration of 1 mM in 1.5 mL Eppendorf tubes. P6 was easily dissolved, but P8 formed a suspension. To make a clear solution of P8, the suspension was sonicated using a bath sonicator. The Eppendorf tubes containing peptide solutions were placed in an EchoTherm model RT11 rotating mixture (Torrey Pines Scientific) with a speed of 50 rpm inside a 37 °C incubator. At suitable time intervals, circular dichroism (CD) spectroscopy and thioflavin T (ThT) fluorescence studies were performed. At the end, electron microscopy (EM), Congo red (CR) absorption, CR fluorescence, and CR birefringence studies were performed (as described below).

**Expression and Purification of p53 Core Domain.** The p53 core domain (residues 94–312) construct, which was generously shared by C. Arrowsmith, was purchased from Addgene (plasmid 24866).<sup>41</sup> p53 core was expressed and purified from *Escherichia coli* host strain BL21(DE3)-(pLys-S) as a fusion protein with an N-terminal His<sub>6</sub> tag according to the protocol of Ayed et al.<sup>41</sup> Briefly, expression of p53 core protein was induced using 1 mM isopropyl  $\beta$ -D-1-thiogalactopyranoside in Luria broth (LB) containing 100  $\mu$ g/mL ampicillin and 34  $\mu$ g/mL chloramphenicol. After being induced at 25 °C for 16 h, cells were harvested and lysed in buffer containing 50 mM

sodium phosphate (pH 8.0), 0.3 M NaCl, 1 mg/mL lysozyme, 15% glycerol, 5 mM  $\beta$ -mercaptoethanol, and 1 mM PMSF. The His<sub>6</sub> tag p53 core protein was purified from the cell lysate using Ni-Sepharose affinity chromatography (GE Healthcare). The purity of the protein was confirmed by a single band in sodium dodecyl sulfate–polyacrylamide gel electrophoresis (SDS–PAGE) and MALDI-TOF analysis (Figure S12A,B of the Supporting Information).

**Circular Dichroism (CD) Spectroscopy.** CD spectroscopy is a useful technique in determining the change in the secondary structure of a protein or peptide during aggregation and amyloid formation.<sup>42,43</sup> For measurement of CD spectra, 16  $\mu$ L of each of the two peptide solutions was diluted in 5% D-mannitol and 0.01% (w/v) sodium azide to a final volume of 200  $\mu$ L such that the final concentration of the peptide solution reached 80  $\mu$ M. In some cases, peptide concentrations of 50 and 100  $\mu$ M were also used to conduct CD spectroscopy. The peptide solutions were placed into a 0.1 cm path-length quartz cell (Hellma, Forest Hills, NY). Spectra were acquired using a JASCO 810 instrument, and measurements were taken at 25 °C. Spectra were recorded over the wavelength range of 198–260 nm. Smoothing of raw data and subtraction of buffer spectra were conducted according to the manufacturer's instructions.

**Thioflavin T (ThT) Fluorescence.** ThT is a dye frequently used to characterize amyloid formation of a protein or peptide, as it binds to amyloid without showing significant binding to the corresponding monomeric protein or peptide.<sup>42–44</sup> To determine the aggregation of protein/peptide samples, a ThT binding experiment was performed. A 1 mM stock solution of ThT in Tris-HCl buffer (pH 8.0) was prepared. Two microliters of this stock solution was mixed with the peptide solution such that final volume reached 150  $\mu$ L and the final peptide concentration reached 50  $\mu$ M. Then the fluorescence was immediately measured. The fluorescence experiments were conducted using a Horiba-JY (Fluoromax 4) spectrofluorometer, with excitation at 450 nm and an emission range of 460–500 nm. The intensity values at 480 nm were plotted. A 10 mm rectangular quartz microcuvette was used for the fluorescence measurements.

**Congo Red (CR) Binding.** Congo red is a dye commonly used to detect amyloids *in vitro* and *in vivo*.<sup>45,46</sup> Similar to ThT, CR binds to the amyloid form of proteins or peptides but not to their monomeric form. This property of CR makes it a suitable dye for characterizing amyloid fibrils.<sup>6,47</sup> Three different techniques were used for the CR binding studies: CR absorbance,<sup>45</sup> CR fluorescence,<sup>6</sup> and CR birefringence.<sup>46</sup> For the CR binding studies, 25 mg of Congo red was dissolved in 100 mL of autoclaved Milli-Q water containing 10% ethanol. It was filtered through a 0.22  $\mu$ m syringe filter and immediately used for the CR binding study. A 15  $\mu$ L CR solution was added to 85  $\mu$ L of D-mannitol containing 50  $\mu$ M P8 and P6. CR absorbance spectra was recorded in the wavelength range of 200–700 nm using a Jasco spectrophotometer (V-650). A 15  $\mu$ L CR solution added to 85  $\mu$ L of a 5% D-mannitol solution, which was used as a control. For CR fluorescence, 15  $\mu$ L of CR was separately added to the 5% D-mannitol solution containing 50  $\mu$ M P6 and P8. The fluorescence was recorded using a Horiba-JY (Fluoromax 4) spectrofluorometer, with excitation at 550 nm and emission recorded in the range of 600–700 nm, keeping a slit widths of 10 nm each. For Congo red birefringence analysis, 1 mg of peptide was dissolved in 100  $\mu$ L of 5% D-mannitol and sonicated for 1 min prior to a 30 min

incubation at room temperature. The solution was centrifuged for 15 min at 12000g to isolate the fibrils. The fibrils obtained were resuspended in autoclaved Milli-Q water by vortexing; 85  $\mu$ L of this solution was mixed with 15  $\mu$ L of a freshly prepared Congo red solution and incubated at room temperature for 5 min in the dark. The solution was again centrifuged at 12000g for 10 min, and the pellet obtained was washed thrice with water to remove the excess CR dye. Finally, the solution was spread evenly onto a glass slide, air-dried at room temperature, and imaged using a microscope (Olympus SZ61 stereo zoom) equipped with two polarizers and a CCD camera.

**In Vitro Seeding Experiment.** Aggregation of a protein or peptide into amyloid fibrils follows a nucleation-dependent polymerization mechanism, which consists of a lag phase in which the protein or peptide slowly forms aggregation-competent fibril nuclei.<sup>48</sup> In this mechanism of aggregation, the preformed fibril seeds reduce the lag time of amyloid formation by the protein or peptide undergoing amyloidogenesis. To analyze whether P8 fibrils seed the aggregation of p53 core domain, an *in vitro* seeding experiment was performed at room temperature. A 100  $\mu$ M stock solution of P8 fibrils was prepared as described above, which was confirmed by ThT binding and electron microscopy. The fibril solution was then sonicated on ice for 3 min at an amplitude of 20% with three pulses “on” and one pulse “off” per cycle. Presonicated P8 fibril seed was added to 400  $\mu$ L of freshly dissolved 10  $\mu$ M p53 core such that final seed concentration reached 1% (v/v) and 2% (v/v), respectively. Five microliters of 1 mM ThT was added to the solution mixture and incubated at 25 °C without agitation. The ThT fluorescence was monitored at regular intervals using a Horiba-JY (Fluoromax 4) spectrofluorometer using an excitation wavelength of 450 nm, and emission was measured in the range of 460–500 nm, with excitation and emission slit widths of 5 nm each. ThT fluorescence intensity values at 475 nm were extracted and plotted versus time. p53 core, 1% seed, and 2% seed alone were also used as controls.

**Transmission Electron Microscopy (TEM).** To analyze the morphology of the protein/peptide aggregates, TEM was conducted. For this, the peptide stock (1 mM) after incubation was diluted to 80  $\mu$ M for electron microscopy and spotted on a carbon-coated Formvar grid (Electron Microscopy Sciences, Fort Washington, PA) and incubated for 5 min at room temperature. For the seeding study, p53 core (in the presence and absence of P8 seeds) at a concentration of 10  $\mu$ M was spotted on a grid. The samples were washed twice with autoclaved distilled water. The samples were then stained with a 1% (w/v) aqueous uranyl formate solution for 5 min, followed by air drying. The images were taken at different magnifications (26000 $\times$ , 43000 $\times$ , and 60000 $\times$ ) at 120 kV using a transmission electron microscope (TECNAI12 D312, FEI).

**Fourier Transform Infrared Spectroscopy (FTIR).** FTIR is frequently used for the determination of protein/peptide secondary structure.<sup>49,50</sup> Previous studies have suggested that FTIR is also useful in detecting the secondary structural transformation during protein aggregation and amyloid formation.<sup>43,51</sup> For FTIR analysis, 5  $\mu$ L of the incubated stock solutions (1 mM) of peptides P6 and P8 and 10  $\mu$ M p53 core protein (both unseeded and seeded) were spotted on thin translucent KBr pellets, kept below the IR lamp, and dried immediately.<sup>52</sup> For the background spectrum, 5  $\mu$ L of 5% D-mannitol was used. The FTIR spectra were acquired as the average of 32 scans at a resolution of 4  $\text{cm}^{-1}$  in the range of 1800–1500  $\text{cm}^{-1}$  by using a Bruker Vertex-80 instrument

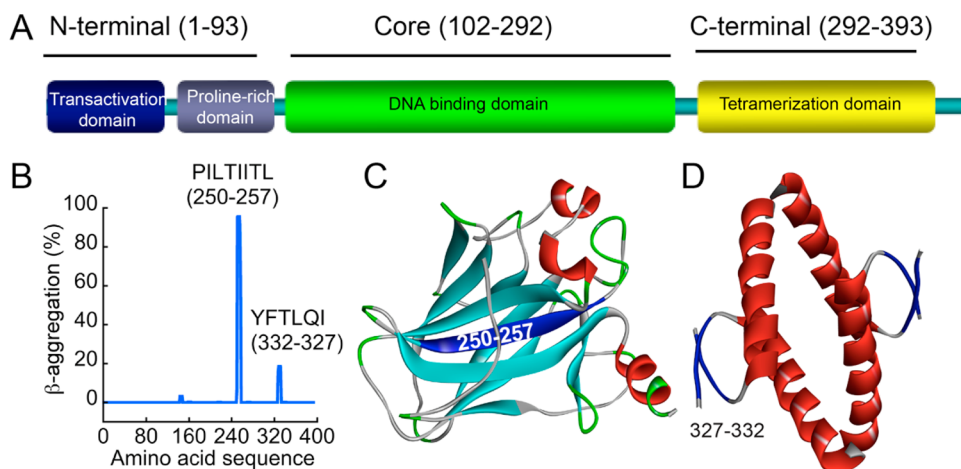


**Figure 1.** Domain organization in p53 tumor suppressor protein. (A) Schematic representation of the different functional domains within p53: the N-terminal domain (residues 1–93), the DNA binding domain (residues 102–192), and the tetramerization domain (residues 292–393). (B) TANGO-predicted  $\beta$ -aggregation-prone regions within the human p53 protein showing two amyloidogenic regions, one within the DNA binding domain (PILTIITL) and the other in the tetramerization domain (YFTLQI). (C) Three-dimensional (3D) structure of the DNA binding domain with the amyloidogenic region (250–257) colored blue (PDB entry 2OCJ). (D) 3D structure of the tetramerization domain with the region colored blue representing amyloidogenic region 327–332 (PDB entry 1AIE).

equipped with a DTGS detector. For secondary structure analysis, the FTIR spectra corresponding to the amide I region ( $1700$ – $1600\text{ cm}^{-1}$ ) were subjected to Fourier self-deconvolution (FSD) followed by a Lorentzian curve fitting procedure in opus-65 software.

**Molecular Dynamics Simulation.** The all atom molecular dynamics (MD) simulation is a vital tool for probing the dynamics of proteins/peptides during folding and aggregation.<sup>43,53–56</sup> In this study, we used MD simulation to probe the aggregation propensities and subsequent secondary structural transitions in two short peptide sequences from the p53 tumor suppressor protein. The two following sequences were probed in this study: (i) region 250–257 with the sequence PILTIITL and (ii) region 327–332 with the sequence YFTLQI. The *in silico* study was performed using conventional MD simulation protocols similar to those used in previous studies.<sup>42,43,56</sup> The initial structures of the two short peptide sequences were obtained from the p53 native protein structures (PDB entry 2OCJ for DBD and 1AIE for TD). The monomeric structures for the two peptides PILTIITL and YFTLQI were energy-minimized, first in vacuum and then via solvation. The solvated peptides were then energy-minimized again, and a molecular dynamics run of 2 ns each was performed on both peptides. The resulting structures were then used as starting structures for the protein aggregation simulation. The peptides were solvated in a TIP3P water box keeping their initial orientations random and then charge-neutralized with  $\text{Na}^+$  and  $\text{Cl}^-$  ions. The two systems were thus set up in the following manner: (i) 24 molecules of PILTIITL in a charge-neutralized water box (labeled A–X) and (ii) 24 molecules of YFTLQI (labeled P1–P24) in a charge-neutralized water box. The two systems were then energy-minimized for 15000 steps using the conjugate gradient algorithm followed by a linear scaled heating from 0 to 310 K. The systems were then equilibrated for 2 ns under *NPT* conditions until the density of the water box reached  $0.98\text{ g/cm}^3$ . The equilibrated system was then used to perform further *NPT* simulations for 65 ns. The equilibration and final dynamics simulation were performed at 310 K and 1 atm of pressure. The van der Waals interaction cutoff used was  $9\text{ \AA}$ , and the electrostatic interaction cutoff was  $12\text{ \AA}$ . All the

simulations were performed using molecular dynamics software package NAMD,<sup>57</sup> and the trajectories were analyzed using VMD.<sup>58</sup>

**Dot Blot Analysis.** To determine the amyloid nature of a protein or peptide, the immunoreactivity of the samples against an amyloid fibril-specific OC antibody<sup>59</sup> and an amyloid oligomer-specific A11 antibody<sup>60</sup> was studied. Two microliters of each sample was spotted on a nitrocellulose membrane and air-dried. The membrane was blocked with 5% skim milk for 1 h at  $25\text{ }^\circ\text{C}$  and then incubated with an anti-amyloid fibril-specific rabbit polyclonal OC antibody (diluted 1:4500, Millipore) and an oligomer-specific rabbit polyclonal A11 antibody (1:5000, Millipore). Blots were treated with an anti-rabbit HRP-tagged secondary antibody (diluted 1:5000, Molecular Probes), and detection was conducted using Super Signal West-Femto Detection reagent (Thermo Scientific). Blots were developed on photographic X-ray film (Kodak).

**In-Cell Seeding and Immunocytochemistry.** SH-SY5Y, a human neuroblastoma cell line, in which p53 is functionally wild-type, was used for the in-cell seeding experiment.<sup>61</sup> SH-SY5Y cells were cultured in Dulbecco's modified essential medium (DMEM) up to  $\sim 80\%$  confluence. After this, cells were treated with  $5\text{ }\mu\text{M}$  prefibrillized unlabeled and/or AlexaFluor647-labeled P8 fibrils for 24 h. Untreated cells were kept as a control. Cells were washed with phosphate-buffered saline (PBS) and fixed with 3.7% paraformaldehyde. Fixed cells were permeabilized using 0.1% Triton X-100 and blocked with 2% bovine serum albumin (BSA) in PBS at  $25\text{ }^\circ\text{C}$ . p53 was immunostained using a 1:300 anti-p53 DO1 primary antibody, sc-126 (Santa Cruz Biotechnology Inc.), and a 1:500 goat anti-mouse FITC-conjugated secondary antibody (Molecular Probes). Cells were mounted with VECTASHIELD mounting medium (Vector laboratories), observed, and imaged under an Olympus FV-500 IX 81 confocal microscope.

## RESULTS

**p53 Sequence Analysis Using Amyloid Predicting Algorithms and Multiple-Sequence Alignment Suggest the Presence of Amyloidogenic Segments within Conserved Regions of p53.** Previously, it has been suggested

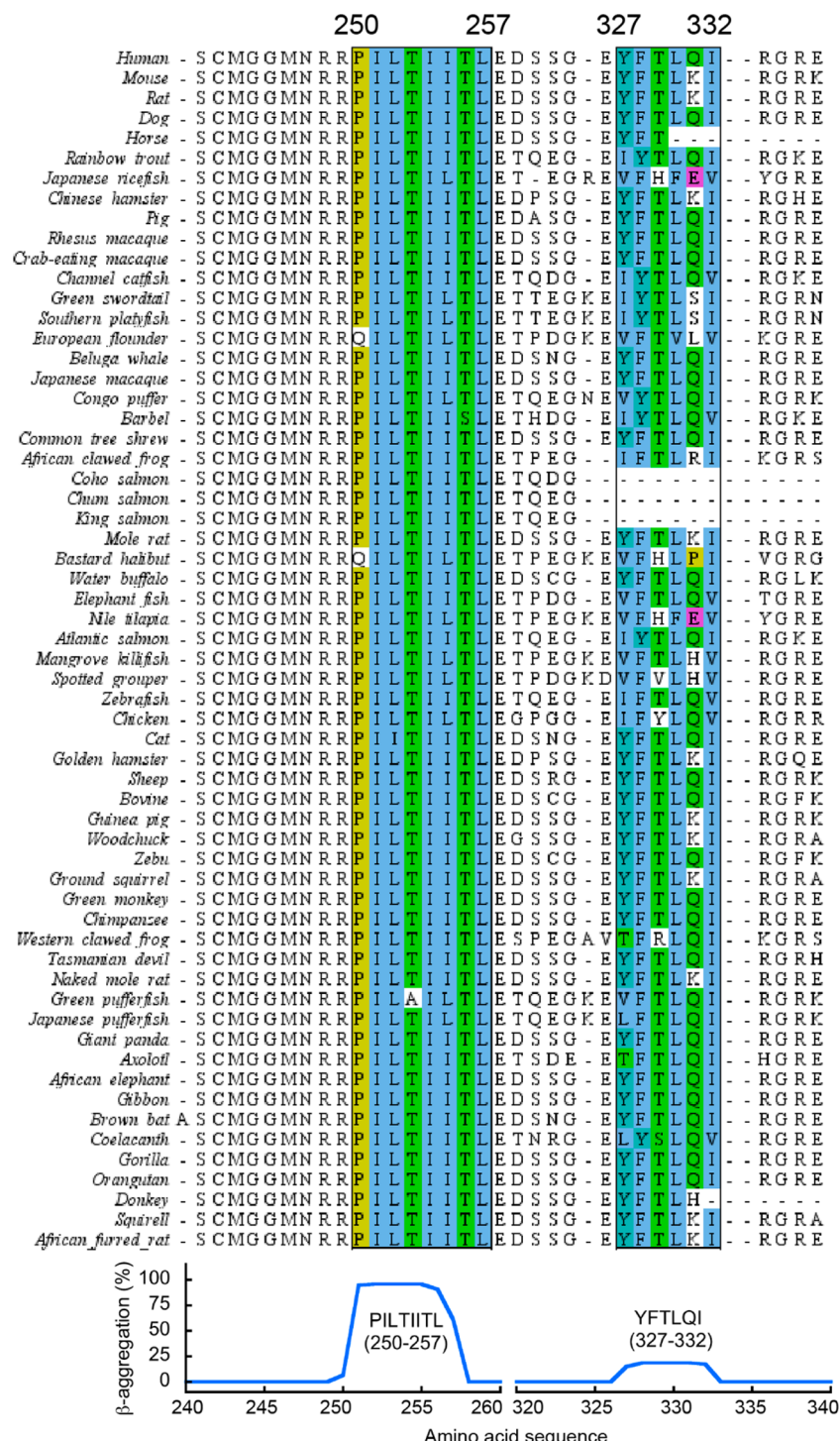


**Figure 2.** Sequence conservation of the two amyloidogenic regions within p53. Multiple-sequence alignment showing a high degree of conservation in the region spanned by residues 250–257 of the DNA binding domain and comparatively less conservation in the region spanned by residues 327–332 of the tetramerization domain. The first sequence (PILTIITL) is found to be present in 57 of 60 organisms chosen for the study, while the second (YFTLQI) was found in only 22 of them.

that p53 can form amyloid *in vitro* and in cancer tissues.<sup>26,27</sup> To understand the amyloidogenicity of p53 protein, we were interested in finding out whether p53 and its family of proteins contain any segment predicted to form amyloid and whether these segments are conserved across different species. Structurally, p53 is organized into three distinct domains (Figure 1A).<sup>62</sup> The unstructured N-terminal domain (NTD) consists of amino acid residues 1–93. The DNA binding core

domain (DBD) consists of residues 102–292 and this is the main domain responsible for interaction with DNA. The C-terminal domain (CTD) comprising residues 293–393 contains a tetramerization domain (TD) and a regulatory domain.<sup>62</sup> When we tested the amyloid prediction of p53 with the TANGO algorithm,<sup>31</sup> we found that two peptide segments corresponding to p53 (250–257) and p53 (327–332) showed amyloidogenic potential with higher amyloid-forming potential

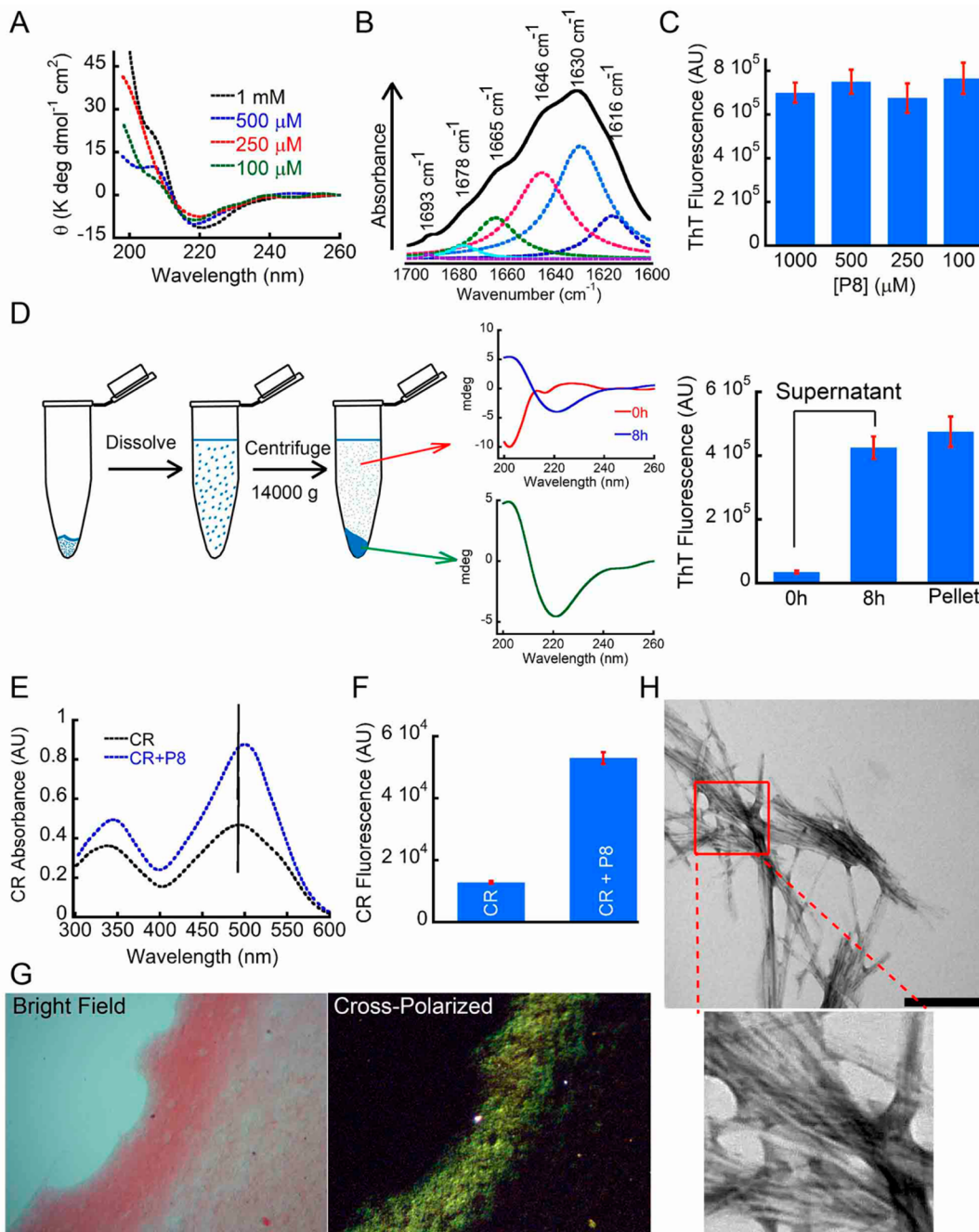


**Figure 3.** Structural transition and aggregation of p53 (250–257) *in vitro*. (A) Circular dichroism spectroscopy of P8 at different concentrations (1 mM, 500  $\mu\text{M}$ , 250  $\mu\text{M}$ , and 100  $\mu\text{M}$ ) showing  $\beta$ -sheet secondary structure. (B) Deconvoluted FTIR spectra of P8 showing  $\beta$ -sheet rich structures corresponding to the peaks at 1616, 1630, and 1693  $\text{cm}^{-1}$  along with the presence of random coil (1646  $\text{cm}^{-1}$ ), 3<sub>10</sub>-helix (1665  $\text{cm}^{-1}$ ), and  $\beta$ -turn (1678  $\text{cm}^{-1}$ ) secondary structures. (C) Thioflavin T binding of P8 showing high ThT fluorescence upon binding at different P8 concentrations (1 mM, 500  $\mu\text{M}$ , 250  $\mu\text{M}$ , and 100  $\mu\text{M}$ ). (D) Schematic representation of solubilization of P8 and the fractions used for CD and ThT binding experiments. P8 was dissolved in 5% d-mannitol and sonicated, leading to the formation of a suspension solution, which was then centrifuged at 14000g for 30 min. The supernatant and pellet fractions were used for CD and ThT binding assays to detect amyloid formation by P8. The supernatant fraction showed a time-dependent structural transition from random coil (0 h) to  $\beta$ -sheet (8 h). (E) Congo red binding showing the increase in molar absorptivity of CR after binding to P8. (F) Increase in Congo red fluorescence intensity upon binding to P8. (G) Light microscope images showing CR binding by P8 under bright-field and cross-polarized light. The latter shows apple-green birefringence characteristic of cross  $\beta$ -sheet rich amyloid. (H) Electron micrograph of P8 showing the fibrillar morphology of amyloids. The inset shows a magnified area of P8 fibrils, in which individual filaments were laterally associated with each other to form dense clusters. Scale bars are 500 nm.

of the p53 (250–257) segment (Figure 1B), which was consistent with previous reports.<sup>29,35</sup> These two segments spanning regions 250–257 and 327–332 had corresponding sequences of PILTIITL and YFTLQL, respectively. Region

250–257 is known to be a part of the DBD of p53, whereas region 327–332 is a part of the TD (Figure 1C,D).

p53 protein is known to be present in most vertebrates, and certain variants of p53 are also found in some invertebrates like the fruit fly *Drosophila melanogaster*<sup>63</sup> and the nematode worm

*Caenorhabditis elegans*<sup>64</sup> and even in bacteriophage APSE-1, which possesses a putative p53-like protein.<sup>65</sup> This shows a functional conservation of p53 protein in spite of millions of years of evolution and speciation. To estimate sequence conservation and/or species-specific variation of p53, we performed multiple-sequence alignment (MSA) of p53 sequences belonging to 60 different species. The species chosen for the study were representative of a large evolutionary time scale. MSA results showed a high level of conservation among organisms belonging to primates and also among various fishes and rodents. MSA also indicated the presence of a highly conserved region spanned by amino acids 126–286 as compared to the other regions (Figure S1 of the Supporting Information). The phylogenetic relationship between the various organisms based upon divergence of p53 is shown in Figure S2 of the Supporting Information. The conserved region is also associated with the DNA binding activity of p53 and is a part of its core domain (Figure 1C).

To assess whether the p53 sequences from other species possess regions with potential aggregation propensity similar to that of human p53, we performed an exhaustive TANGO and WALTZ analysis of 60 different species (Table S15 of the Supporting Information). The number of regions predicted to have  $\beta$ -aggregation propensity varies among various species. Results of the TANGO algorithm range from species predicted to have only one amyloidogenic region, such as *Equus asinus* (donkey) and *Spermophilus tridecemlineatus* (thirteen-lined ground squirrel), to species that might have as many as five regions with amyloid forming propensity, such as *Callorhynchus milli* (elephant fish) (Figure S3 of the Supporting Information). WALTZ analysis of p53 sequences from 60 species, performed using a threshold of “best overall performance”, also showed a variation in the number of potential hot spots of aggregation (Table S15 of the Supporting Information). Sequence alignment data also reflect the high degree of conservation of these two putative aggregation-prone sequences (P1 and P2). When we analyzed these two segments for their extent of conservation across different species, we found that the sequence PILTIITL was present in 57 of the 60 studied species with minor point variations in the other three. On the other hand, the sequence YFTLQI, which is a part of the tetramerization domain (TD) of p53, was relatively less conserved; it was found in only 22 species with random variations in others. This segment was totally absent from five species. The degree of conservation of these two regions is depicted in Figure 2. The amyloidogenic regions within p53 protein from various organisms and their respective amyloidogenic propensities (in percentage) are listed in Table S15 of the Supporting Information. The average  $\beta$ -aggregation propensity predicted for PILTIITL was 95.5%, and that for YFTLQI was 18% according to the TANGO algorithm. These results were corroborated using other aggregation prediction algorithms like AGGRESCAN, WALTZ, PASTA, and Zipper DB (Figure S14 of the Supporting Information). The data suggest that p53 is highly amyloidogenic, as reported by previous aggregation prediction studies,<sup>35</sup> and showed that p53 contains a primary amyloidogenic segment in its DBD/core domain and an additional aggregation-prone region in the tetramerization domain (TD).

**Conformational Transition and Amyloid Formation by p53 (250–257) *in Vitro*.** Because of the conserved nature of p53 region 250–257 (PILTIITL) across different species, which was also predicted to be highly amyloidogenic by the TANGO algorithm, we were interested in studying the

aggregation behavior of this segment *in vitro*. Therefore, P8 (peptide representing PILTIITL) was synthesized by the solid-phase peptide synthesis method, and a >98% pure peptide was used for the study. The peptide was dissolved at a concentration of 1 mM in 5% d-mannitol and 0.01% sodium azide (pH 5.5) and incubated at 37 °C. CD spectra were analyzed to elucidate the secondary structure of the peptide *in vitro*.<sup>66</sup> P8 formed a suspension solution immediately upon dissolution, probably because of its highly hydrophobic character. To solubilize the peptide, the peptide suspension was sonicated for 5 s using a bath sonicator that resulted in a clear and suspension-free solution. Interestingly, immediately after sonication and dissolution, CD spectra of P8 showed  $\beta$ -sheet secondary structure characterized by single minima at ~218 nm. To rule out the possibility that a higher concentration (1 mM) was responsible for P8's rapid structural transition to  $\beta$ -sheet, lower concentrations of P8 (500, 250, and 100  $\mu$ M) were prepared. However, all of the samples showed characteristic  $\beta$ -sheet secondary structure via CD spectroscopy (Figure 3A). The conformation of aggregates was further probed using FTIR spectroscopy.<sup>67</sup> The 1 mM samples of P8 primarily showed  $\beta$ -sheet rich structures corresponding to the peaks at 1616, 1630, and 1693  $\text{cm}^{-1}$  (Figure 3B). Additionally, P8 also showed the occurrence of random coil (1646  $\text{cm}^{-1}$ ), 3<sub>10</sub>-helix (1665  $\text{cm}^{-1}$ ), and  $\beta$ -turn (1678  $\text{cm}^{-1}$ ) secondary structures. ThT fluorescence was used to monitor amyloid formation.<sup>52</sup> The P8 solution at all concentrations studied (100  $\mu$ M to 1 mM) showed a high level of ThT binding. The data suggest that P8 formed amyloid immediately at all these peptide concentrations (Figure 3C). The rapid formation of  $\beta$ -sheet structure and the absence of random coil could be due to the strong tendency of P8 to form amyloid, and/or sonication might have accelerated the aggregation kinetics. To verify this observation, we prepared a P8 solution in 5% d-mannitol and vortexed it, which resulted in a suspension solution. This solution was then centrifuged at 14000g for 30 min, and the supernatant and pellet fractions were separated. The schematic in Figure 3D represents the experimental plan followed for dissolving P8 and analyzing its secondary structural transition *in vitro*. CD spectra of the pellet fraction showed  $\beta$ -sheet secondary structure (Figure 3D), which also showed a high level of ThT binding, confirming amyloid formation. The supernatant fraction showed mostly random coil conformation, and upon incubation for 8 h, this fraction showed a structural transition to  $\beta$ -sheet secondary structure with an increase in the level of ThT binding (Figure 3D).

To ascertain the amyloid formation of peptide P8, Congo red (CR) binding was performed. CR is another dye frequently used for amyloid detection *in vitro* and *in vivo*.<sup>6,45,47</sup> Three different techniques (CR absorbance, CR fluorescence, and CR birefringence) were used to confirm the amyloid formation by P8. After addition of CR to P8 aggregates, increases in the molar absorbance and CR fluorescence intensity were observed (Figure 3E,F). The binding of CR to P8 amyloids was further confirmed by the classical CR birefringence analysis.<sup>46,47</sup> Upon binding with CR, P8 showed an apple-green birefringence, a characteristic of amyloids (Figure 3G). Aiming to characterize the morphology of the aggregates formed by P8, we further subjected the incubated P8 peptide to electron microscopy. Electron micrographs revealed the fibrillar morphology of the P8 aggregates. The fibrils formed were seen to be very thin, straight, and laterally associated with each other, forming highly dense clusters (Figure 3H and inset). Overall, our results

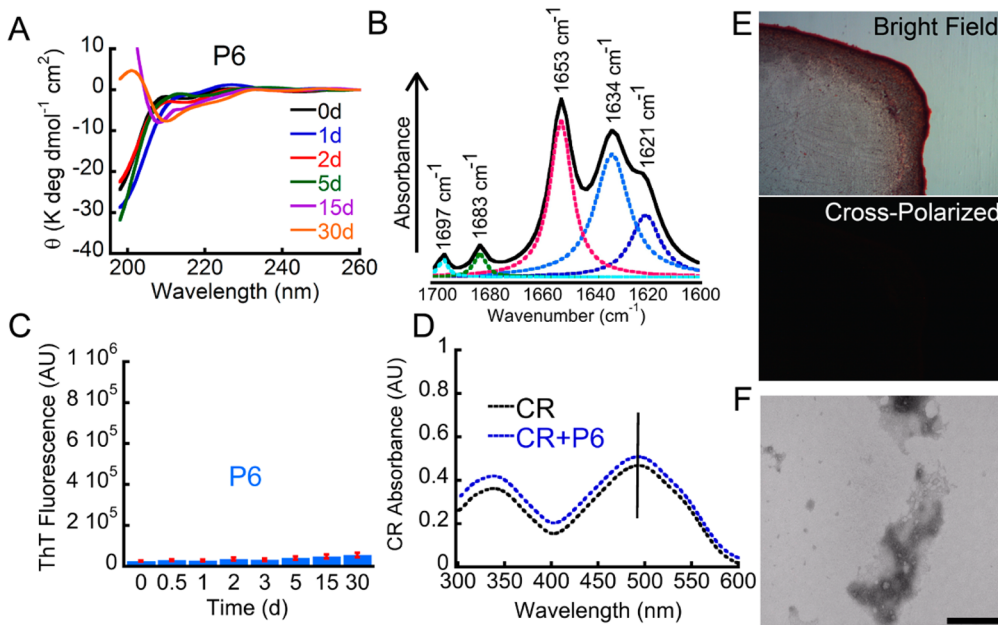


**Figure 4.** p53 (327–332) is nonamyloidogenic *in vitro*. (A) CD spectra showing the conformational transition of P6. (B) Deconvoluted FTIR spectra of preincubated P6 showing the occurrence of  $\alpha$ -helix rich structure as seen by an intense peak at  $1653\text{ cm}^{-1}$  accompanied by the presence of  $\beta$ -sheet (peaks at  $1621$ ,  $1634$ , and  $1697\text{ cm}^{-1}$ ) and  $\beta$ -turn (peak at  $1683\text{ cm}^{-1}$ ) structures. (C) ThT fluorescence of P6 showing very weak binding of ThT to P6. (D) Negligible change in CR molar absorptivity upon binding to P6. (E) Light microscopy images of CR binding to incubated P6 under bright-field and cross-polarized light. P6 does not show the typical birefringence behavior of amyloids. (F) Electron micrographs of P6 aggregates showing amorphous nonamyloid accumulations. Scale bars are 500 nm.

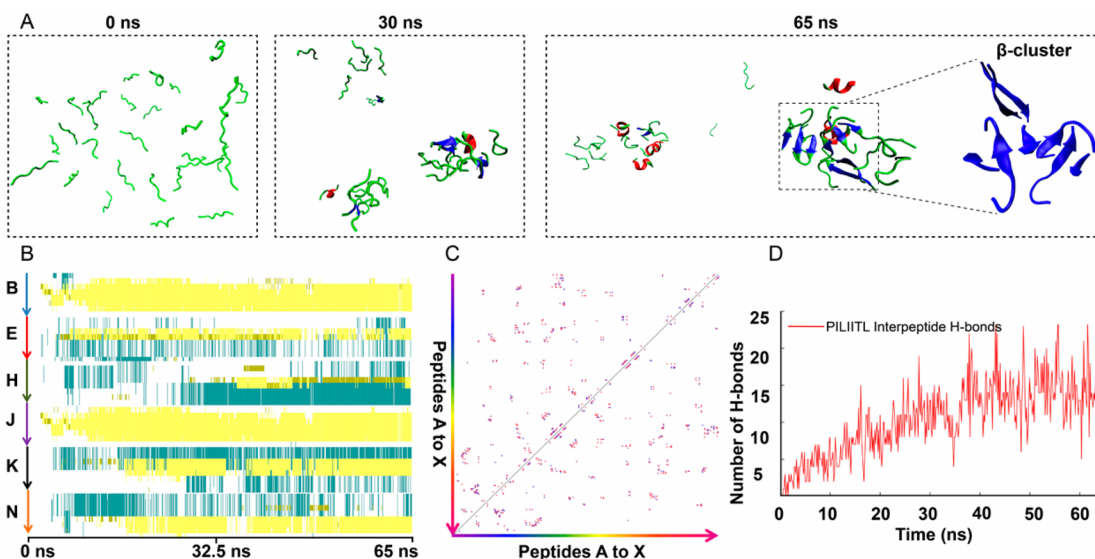


**Figure 5.** Characterizing p53 (250–257) self-association and secondary structural progression. (A) Snapshots of the PILIIITL system at three different time points (0, 30, and 65 ns) during the simulation showing the self-association and conformational transition of peptides. After simulation for 65 ns, the observed  $\beta$ -sheet rich aggregate is highlighted. The  $\beta$ -sheets are colored blue, while helical structures are colored red. (B) Secondary structural transition of selected peptides transforming into  $\beta$ -sheet (peptides B, E, H, J, K, and N) during the 65 ns simulation. White, green, blue, pink, and yellow indicate random coil, turn,  $\pi$ -helices,  $\alpha$ -helices, and  $\beta$ -strand, respectively. (C) Contact map of PILIIITL peptides at 65 ns showing various interpeptide contacts formed during the 65 ns simulation. Colored dots on either side of the diagonal represent non-self-contacts, while the diagonal represents self-contacts. (D) Interpeptide hydrogen bonding of PILIIITL peptides during the simulation showing the increase in the number of hydrogen bonds over time.

suggest that P8 is amyloidogenic in nature and can assemble into higher-order amyloid aggregates.

**p53 (327–332) Does Not Aggregate into Amyloid.** To study the aggregation and amyloid formation by peptide sequence corresponding to p53 (327–332, P6), the peptide was also synthesized using the solid-phase peptide synthesis

method and purified by high-performance liquid chromatography to >98% purity. The mass of the peptide was also confirmed by MALDI-TOF mass spectroscopy. P6 was dissolved at a concentration of 1 mM in 5% D-mannitol and 0.01% sodium azide (pH 5.5) and incubated at 37 °C. P6 dissolved readily, unlike P8. The CD study suggested that

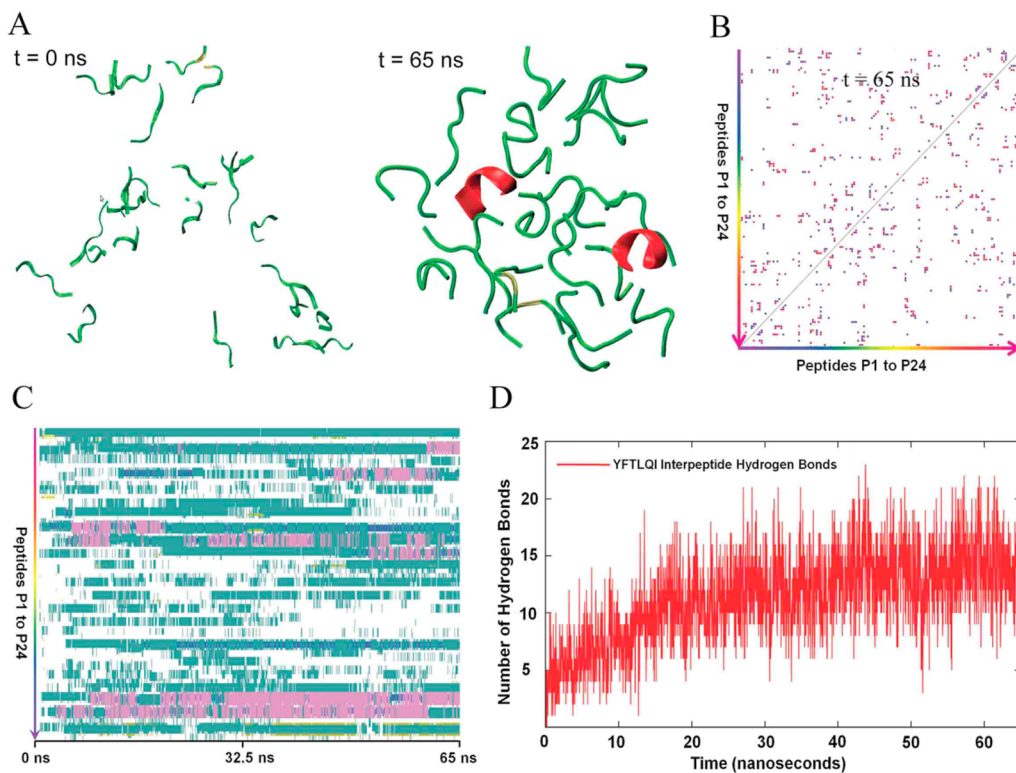


**Figure 6.** MD simulation of YFTLQI peptides. (A) Initial (left) and final (right) configurations of the YFTLQI peptide displaying the self-association of YFTLQI peptides into aggregates with mostly RC structures. (B) Contact map of YFTLQI peptides at 65 ns showing various interpeptide contacts formed during the 65 ns simulation. Colored dots on either side of the diagonal represent non-self-contacts, while the diagonal represents self-contacts. (C) Secondary structural progression of YFTLQI during the simulation. White, green, blue, pink, and yellow indicate random coil, turn,  $\pi$ -helices,  $\alpha$ -helices, and  $\beta$ -strand, respectively. (D) Interpeptide hydrogen bonding during simulation showing the increase in the number of hydrogen bonds with time.

immediately after dissolution, P6 mostly adopts a random coil secondary structure, represented by a single minimum at 198 nm. It did not show any structural change after being incubated for up to 5 days (Figure 4A). However, after being incubated for 15 days, it adopted a helical secondary structure characterized by two minima at  $\sim$ 208 and  $\sim$ 222 nm. The solution was incubated for a longer period to observe any further secondary structural changes. Even after being incubated for 30 days, P6 retained its helical structure. FTIR spectra of incubated samples of P6 showed the presence of  $\alpha$ -helix rich structure characterized by the most intense peak at  $1653\text{ cm}^{-1}$  (Figure 4B). However, it also showed some amount of  $\beta$ -sheet structure corresponding to the peaks at 1621, 1634, and  $1697\text{ cm}^{-1}$ . The peak at  $1683\text{ cm}^{-1}$  indicates the presence of a certain amount of  $\beta$ -turn. Electron microscopy revealed that P6 formed nonfibrillar amorphous aggregates characteristic of a nonamyloidogenic protein or peptide (Figure 4F). ThT of P6 showed insignificant binding immediately after dissolution, and after incubation for 30 days, no significant increase in the level of ThT binding was observed, suggesting the absence of amyloid formation by P6 (Figure 4C). Aggregation and amyloid formation were further analyzed by CR binding using the CR absorbance and birefringence method. Neither a significant increase in CR molar absorbance nor apple-green birefringence was observed for the incubated P6 sample (Figure 4D,E). The biophysical study suggests that P6 did not form amyloid *in vitro* irrespective of the aggregation potential (although it was low compared to that of P8) observed from TANGO analysis.

**p53 (250–257) Shows a Structural Transition to  $\beta$ -Sheet Structures *in Silico*.** To probe the aggregation of p53 250–257 (PILTIITL) in residue-specific detail, we performed all atom MD simulation of the peptide in explicit solvent with 24 molecules of P8 in a solvent box. Snapshots of the PILTIITL system at various time points during the simulation are shown in Figure 5A and Figure S4 of the Supporting Information. While the peptides remained mostly unassociated and monomeric initially, the development of various self-associated clusters was apparent as the simulation progressed. Interestingly, the PILTIITL peptide not only showed the ability to self-assemble but also displayed a significant tendency to undergo a secondary structural transition from random coil-like structures to  $\beta$ -sheet rich aggregates. This is evident from the 65 ns simulation, where the earliest traces of  $\beta$ -sheet signatures were apparent as early as 10 ns (Figure S4 of the Supporting Information). The initially formed  $\beta$ -sheets remained stable until the end of the study. The secondary structural progression of selected peptides, those that showed a transition from random coil to the  $\beta$ -sheet configuration, is represented in Figure 5B. However, the secondary structural transition of the entire system is shown in Figure S5 of the Supporting Information, representing the conformations accessed by all the P8 peptides during the simulation. Crucially, the development of a stable predominantly  $\beta$ -sheet rich cluster was evident toward the latter part of the simulation ( $\sim$ 50–65 ns). This self-assembled cluster of  $\beta$ -sheet structures showed a mixture of parallel and antiparallel  $\beta$ -sheets. A detailed look at one of the major  $\beta$ -sheet aggregated structures formed during the

simulation is also shown in Figure 5A. This strong tendency to not only self-associate but also undergo a structural transition to  $\beta$ -sheet-like structures even on very early time scales thus strongly indicates the amyloidogenic potential of this sequence within the DBD of p53. We further analyzed the interpeptide contact during the simulation. The data showed negligible interpeptide contacts at the start of the simulation (Figure S6A of the Supporting Information), which increased considerably after simulation for 65 ns, as represented by the dots on either side of the diagonal in the contact map in Figure 5C. An increased level of self-association was also accompanied by an increase in the level of interpeptide hydrogen bonding during the duration of the simulation as shown in Figure 5D. The most frequently observed hydrogen bonds (which exist for >50% of the simulation time) are summarized in Table S16 of the Supporting Information. The data suggest that residues Leu<sup>252</sup>, Thr<sup>253</sup>, Ile<sup>254</sup>, Ile<sup>255</sup>, and Leu<sup>257</sup> were found to be the most frequently involved in hydrogen bonding, stabilizing the  $\beta$ -sheets formed by PILTIITL peptides.

Further, the root-mean-square deviation (rmsd) plot suggests that the system undergoes an initial period of fluctuations where the peptides assemble into self-associated clusters (Figure S6B of the Supporting Information). The system then stabilizes following the formation of these clusters. The radii of gyration of the peptides during the simulation also advocate the system having reached stability after the 65 ns simulation (Figure S7 of the Supporting Information).

#### p53 (327–332) Shows a Minimal Structural Transition during the 65 ns Simulation Even after Self-Association.

To further probe the aggregation of P6, which showed a weaker tendency to aggregate predicted by TANGO (Figure 1B) and did not show any amyloid formation *in vitro* (Figure 4), we performed an all atom simulation using 24 peptides of P6 in the explicit water. The detailed progression of the 24-peptide P6 system is shown in Figure S8 of the Supporting Information, where the peptides undergo a transition from an initial monomeric state to a self-assembled state at the end of the simulation. The peptides showed aggregation into a single self-associated cluster (around 30 ns) and remained stable until the end of the simulation. The initial and final configurations of the YFTLQI system clearly reveal the self-association of P6 (Figure 6A). The analysis of interpeptide contacts formed by 24 P6 at the beginning of the simulation (Figure S10A of the Supporting Information) and at the end of the 65 ns simulation (Figure 6B) revealed that very few interpeptide contacts were present between the peptides initially (Figure S10A of the Supporting Information). However, an increase in the number of interpeptide contacts during the 65 ns simulation was observed (Figure 6B). An overview of the secondary structural conformations (Figure 6C) assumed by all the peptides during the simulation suggests a negligible conformational transition of the P6 system. However, few of the peptides showed a transition to the helical state. The secondary structure progression of each peptide (peptides P1 and P24) during the simulation is shown in Figure S9 of the Supporting Information. The analysis of interpeptide hydrogen bonds showed an increase in the level of interpeptide hydrogen bonding during the simulation (Figure 6D). The rmsd progression data suggest that the system stabilized after an initial period of arrangement and self-association (Figure S10B of the Supporting Information). The radii of gyration ( $R_g$ ) of YFTLQI peptides during the simulation showed that the peptides remained stable or showed a sharp decrease in the case

of some of the peptides; those peptides showed a tendency to assume a helical conformation (Figure S11 of the Supporting Information).

**Arginine Substitution and Residue Shuffling Abolish the Amyloidogenic Potential of p53 (250–257).** The analysis of the MD simulation data of p53 (250–257) revealed that residues Leu<sup>252</sup>, Ile<sup>254</sup>, Ile<sup>255</sup>, and L<sup>257</sup> are most frequently involved in H-bonding during the self-aggregation of this peptide *in silico*. Therefore, we intended to study the aggregation of the native p53 (250–257) segment with one or more of the four residues listed above substituted with Arg, an amyloid gatekeeper amino acid.<sup>32</sup> We designed and chemically synthesized two peptides, PIRTIITL and PIRTRRRTL, with multiple substitutions of Leu<sup>252</sup>, Ile<sup>254</sup>, Ile<sup>255</sup>, and Leu<sup>257</sup> (Figure 7A). Interestingly, the TANGO

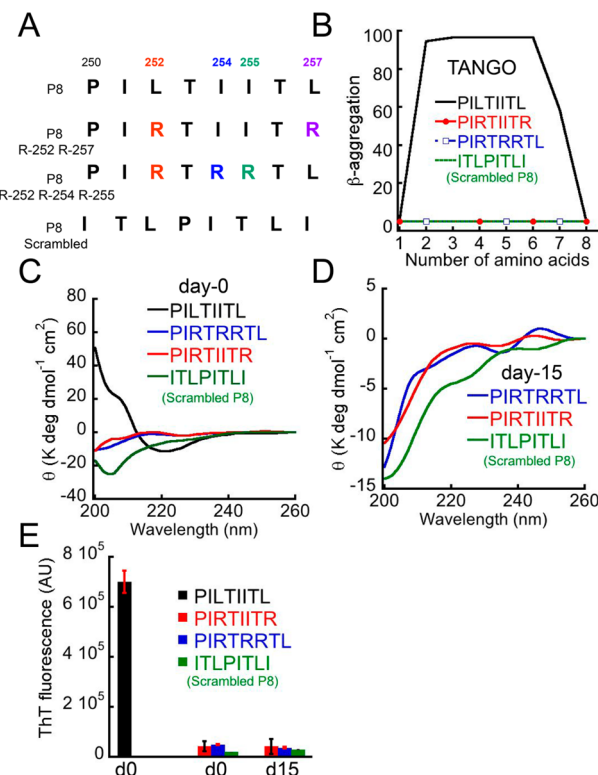


**Figure 7.** Arginine substitution and residue shuffling abolish the amyloid potential of p53 (250–257). (A) Amino acid sequences of p53 (250–257) (PILTIITL), the Arg-substituted peptides, PIRTIITL and PIRTRRRTL, and the scrambled peptide, ITLPITLI (Scrambled P8). (B) TANGO prediction showing elimination of amyloidogenic potential of the arginine-substituted and scrambled peptides. (C) CD spectra of native, Arg-substituted, and scrambled p53 (250–257) peptides immediately after dissolution and (D) after incubation for 15 days, showing a lack of structural transition in both the Arg-substituted and scrambled peptides. (E) ThT binding data showing the inability of Arg-modified segments and scrambled peptide to aggregate into amyloid.

analysis of these two modified peptides showed complete diminution of the  $\beta$ -aggregation propensity of the peptides (Figure 7B). Both of these modified peptides showed random coil secondary structure immediately after dissolution (Figure 7C), which did not change even after incubation for 15 days (Figure 7D). The ThT binding study also showed that both of these peptides did not bind ThT (Figure 7E), suggesting that Arg substitution of key contact residues (deduced from our MD results) eliminated amyloid formation by the P8 peptide.

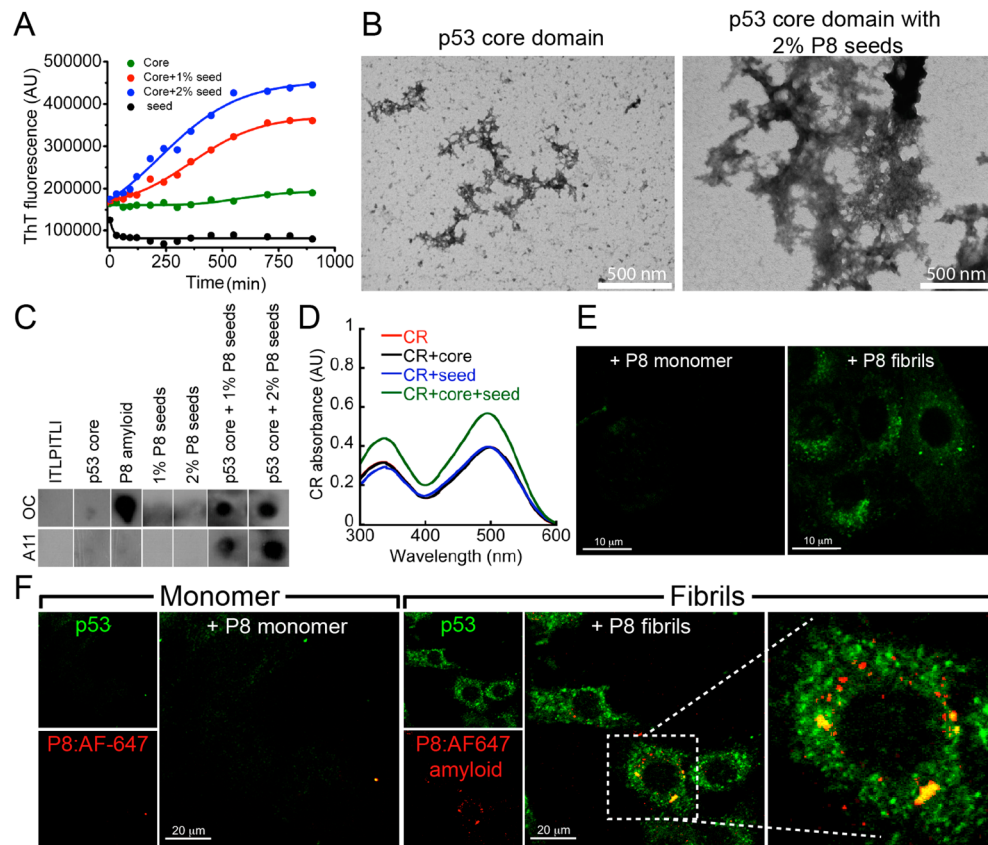


**Figure 8.** Seeding effect of p53 (250–257) fibrils on the aggregation of p53 core domain *in vitro* and native p53 in cells. (A) Kinetics of p53 core aggregation seeded by 1 and 2% presonicated P8 fibrils as monitored by ThT binding. The seeding experiment was performed at room temperature. p53 core or P8 seeds alone do not show any increase in the level of ThT binding with time. (B) Morphology of the aggregates of unseeded p53 core and p53 core seeded with 2% P8 fibril seeds determined by electron microscopy. Denser aggregates were observed in the case of the seeded p53 core. The scale bar is 500 nm. (C) Immunoblot of scrambled P8 peptide ITLPITLI, p53 core, P8 amyloid, 1 and 2% diluted P8 seeds (v/v), and the p53 core with 1 and 2% seeds using the anti-amyloid fibril OC antibody and the anti-oligomer A11 antibody. P8 amyloid and p53 core incubated with 1 and 2% P8 seeds show strong OC and A11 immunoreactivity. (D) Congo red absorbance of the seeded p53 core. (E) Seeding activity of 5  $\mu$ M unlabeled P8 on native full-length p53 in SH-SY5Y cells. Aggregates of p53 are observed as green punctate cytoplasmic structures. Cells with monomeric P8 added show negligible p53 staining. The scale bar is 10  $\mu$ m. (F) Seeding of full-length p53 (green) by AlexaFluor647-labeled P8 fibrils (red) in cells. The magnified image shows colocalization of internalized labeled P8 fibrils with cytoplasmic p53 aggregates.

To further ascertain the importance of sequence specificity of P8 (PILTIITL) for its aggregation, a scrambled peptide (ITLPITLI) was designed. TANGO analysis did not display any predicted  $\beta$ -aggregation tendency of the scrambled peptide (Figure 7B). Upon dissolution, the scrambled ITLPITLI peptide showed random coil secondary structure by circular dichroism spectroscopy analysis (Figure 7C), which persisted even after incubation for 15 days (Figure 7D). Binding of ThT dye by the scrambled ITLPITLI peptide was negligible even after incubation (Figure 7E), suggesting that this peptide is unable to form any amyloid-like aggregates as predicted by TANGO analysis.

**p53 (250–257) Fibrils Seed the Aggregation of p53 Core Domain *In Vitro* and Native p53 in Cells.** To determine whether the p53 (250–257) amyloid fibrils can recognize and interact with their identical sequence in the p53 protein and possibly drive its aggregation, we performed seeding experiments *in vitro* and in cultured cells. Using diluted preformed P8 fibrils, which were sonicated to generate smaller fibril fragments (P8 fibril seeds), we performed a seeding experiment with the recombinantly expressed p53 core domain (Figure 8A). The p53 core domain possesses most of the cancer-associated mutations and is known to retain DNA

binding activity.<sup>68,69</sup> The isolated core domain has also been shown to form aggregates similar to those of full-length p53.<sup>26,30</sup> The SDS-PAGE and MALDI-TOF data of the purified p53 core protein are provided in Figure S12A,B of the Supporting Information. The purified recombinant p53 core domain (10  $\mu$ M) was incubated with 1 and 2% P8 seeds (v/v) at room temperature, and protein aggregation was monitored using ThT fluorescence. We observed that both 1 and 2% seeds induced aggregation of the p53 core in a concentration-dependent manner as shown by their high level of ThT binding during incubation. The p53 core protein and P8 seeds by themselves did not show any significant ThT binding throughout the experiment. The data revealed a high seeding potential of the P8 amyloid fibrils.

We further analyzed and compared the morphologies of the p53 core and seeded p53 core protein via electron microscopy to detect any visible morphological changes (Figure 8B). It was interesting to observe that seeded aggregates of the p53 core were extensively denser and of higher order as compared to those of the unseeded protein. Although the classical feature of amyloid fibrils was not seen in seeded aggregates of the p53 core via EM, the ThT binding data indicate the amyloidogenic nature of the aggregates. To further verify whether seeded

aggregates of the p53 core possess an amyloid fibril-like conformation, we conducted dot blot analysis using amyloid-specific antibodies OC and A11 and CR dye binding studies. Among all the samples tested, undiluted P8 amyloid (positive control) showed positive immunoreactivity with the OC antibody but not with the anti-oligomer A11 antibody, specifying the presence of the fibrillar conformation and the absence of the prefibrillar oligomeric conformation in P8 amyloid. The p53 core incubated with 1 and 2% seeds showed positive immunoreactivity with both OC and A11 antibodies, indicating the presence of both amyloid fibril and prefibrillar oligomeric aggregates (Figure 8C and Figure S12C of the Supporting Information). The individual 1 and 2% seed samples and unseeded p53 core, which were used as controls, showed negligible OC and A11 immunoreactivity. Scrambled P8 (negative control) did not show any OC or A11 immunoreactivity. Similarly, in the CR binding assay, the seeded aggregates of the p53 core showed CR absorbance at 500 nm higher than that of the incubated p53 core alone and P8 seeds (Figure 8D). CR dye in buffer was used as a control.

To determine the effect of seeding on the secondary structural transition in the p53 core protein by P8 fibrils, we performed FTIR spectroscopy. FTIR analysis of the unseeded p53 core protein (freshly purified) showed  $\beta$ -sheet secondary structure corresponding to the peaks at 1618 and 1637  $\text{cm}^{-1}$  and  $\beta$ -turn structure as evident from the peak at 1685  $\text{cm}^{-1}$  (Figure S13 of the Supporting Information). In addition, there was a significant peak at 1653  $\text{cm}^{-1}$  representing  $\alpha$ -helical secondary structure. On the other hand, FTIR analysis of the seeded p53 core sample showed an overall increase in  $\beta$ -sheet content as represented by robust peaks at 1624 and 1637  $\text{cm}^{-1}$ . Moreover, there was a compensatory reduction in the  $\alpha$ -helical and  $\beta$ -turn secondary structural content of the seeded sample. These data are consistent with previous findings, which suggest that upon aggregation, the p53 core shows a higher amount of  $\beta$ -sheet conformation than that of soluble p53 as ascertained by our FTIR study.<sup>26,29</sup> Therefore, our FTIR data are in strong agreement with our interpretation of the ThT and CR dye binding experiments that P8 fibril seeds template the aggregation of the p53 core into  $\beta$ -sheet rich higher-order aggregates.

Recently, it has been shown that p53 aggregates can also seed the aggregation of native, functional p53<sup>26,35,36</sup> and other cellular proteins (such as p53 paralogs, p63 and p73),<sup>29</sup> leading to gain-of-function effects by inducing oncogenic properties in cells. To test whether P8 amyloid can seed native full-length p53 in cells, we added 5  $\mu\text{M}$  P8 fibrils to the growth medium of cultured SH-SY5Y neuroblastoma cells. After the cells had been cultured for 24 h, we immunostained the fixed cells to visualize the status of p53. As a control, we used P8 monomers. It has been suggested that p53 has a short half-life in cells and therefore cannot be detected by immunostaining.<sup>13</sup> However, in cells treated with P8 fibrils, positive immunostaining of p53 was observed and p53 was mostly localized in the cytoplasm. The punctate nature of the cytoplasmic inclusions of p53 suggests that P8 fibrils seed the aggregation of native full-length p53 into large protein aggregates (Figure 8E). On the other hand, in cells treated with P8 monomers, we did not observe any significant p53 signal. In a similar experiment, Alexa-Fluor647-labeled P8 (red fluorescence) was used, and we obtained a visual confirmation of the internalization of P8 fibril seeds and their localization in the cytoplasm (Figure 8F). Colocalization signals between labeled P8 (red) and cellular

p53 (green) indicated that P8 fibrils may interact with its identical sequence in native cellular full-length p53 and seeded its aggregation. A magnified version of a cell showing internalized P8 and p53 aggregates in punctate form is shown for better visual interpretation (Figure 8F).

## ■ DISCUSSION

The tumor suppressor function of p53 is dependent on its structure and its localization in the nucleus, where it binds to its cognate DNA sequence and triggers the expression of various genes responsible for the maintenance of genome stability.<sup>9,11</sup> Although, in normal cells, p53 levels are tightly regulated resulting in its short half-life (15–30 min),<sup>12,13</sup> most point mutations in any of the three domains of p53 (NTD, DBD, and TD) prolong the half-life of p53, leading to cytoplasmic and/or nuclear inclusions.<sup>13,29</sup> The DBD of p53 contains 97% of cancer-related missense mutations,<sup>70</sup> and these mutations lead to its loss of function either by changing the conformation of the DBD or by decreasing the overall thermodynamic stability of the protein. The most frequent cancer-related mutations occur in six hot spot amino acid residues of p53 (residues 175, 245, 248, 249, 273, and 282), which are located in the DBD of the protein.<sup>71</sup> Mutations in the p53 DBD may be responsible for the structural destabilization of the protein and/or loss of its DNA binding ability, both of which can result in a loss of antitumor functions of p53.<sup>72,73</sup> Many hot spot mutations have been found to increase the level of accumulation of p53 in both the cytoplasm and nucleus,<sup>13,26,29</sup> suggesting that mutations can induce aggregation in both compartments. Moreover, cytoplasmic sequestration of wild-type p53 protein has been observed in a subset of primary human tumors, including breast cancer, colon cancer, and neuroblastoma (NB).<sup>16,18–20</sup> Several recent *in vitro* and *in-cell* studies indicate that p53 loss of function could also be due to the aggregation and amyloid formation by wild-type, cancer-associated mutant and zinc-depleted p53 (apo-p53).<sup>21,24–26</sup> The aggregation of p53 may occur in the nuclear and cytoplasmic compartments of the cell.<sup>16,26</sup> p53 aggregation in the cytoplasm may hinder its transport to the nucleus, thereby causing a loss of p53's function as a transcription factor.<sup>35,74–76</sup> On the other hand, the nuclear aggregates of p53 may either be incapable of interacting with p53's consensus DNA binding site,<sup>28,25</sup> or those aggregates might aberrantly interact with DNA, driving the transcription of genes with undesirable functions.<sup>77</sup> The cytoplasmic p53 aggregates may further not only interact with their native protein counterpart and drive their aggregation similar to prion-like seeding mechanism<sup>26,35,36</sup> but also sequester the p53 paralogs, p63 and p73, which might make cells vulnerable to tumor-inducing stress.<sup>29</sup> Therefore, understanding the mechanism of p53 loss of function and knowledge of regions in p53 responsible for its aggregation and amyloid formation is an important aspect of tumor cell biology.

Our MSA study showed that the DBD of p53 from all the organisms under study is mostly conserved through evolution (Figure S1 of the Supporting Information), signifying its important role in aiding the protein's normal cellular functions. When aggregation prediction was conducted using the TANGO algorithm (Figure S3 of the Supporting Information), the data showed that p53 from different organisms contain more than one aggregation-prone segment. The human p53 protein from the TANGO analysis showed two putative aggregation-prone sequences, region 250–257 in the DBD and region 327–332 in the TD (Figure 1B), consistent with

previous studies.<sup>29,35</sup> Similar to TANGO, when p53 from 60 different species were studied using the WALTZ algorithm,<sup>33</sup> a variable number of putative aggregation-prone stretches were identified in those species (Table S15 of the Supporting Information). Human p53 showed seven hot spots of aggregation along with p53 (250–258), when analyzed by WALTZ using a threshold of “high sensitivity” (Figure S14C of the Supporting Information). The aggregation propensities of p53 were further analyzed using AGGRESCAN, PASTA, and Zipper DB, all of which further confirmed the high aggregation propensities of p53, consistent with previous aggregation analysis (Figure S14 of the Supporting Information).<sup>35,36</sup> AGGRESCAN analysis of human p53 revealed eight major hot spots for aggregation, including one amyloidogenic region, p53 (251–257), ILTIITL segment (Figure S14B of the Supporting Information). AGGRESCAN analysis also shows an aggregation hot spot in the p53 tetramerization domain spanning residues 327–332, the YFTLQI region. The aggregation analysis by all algorithms validated that among other hot spots of aggregation in p53, region 250–257 was the most commonly identified amyloidogenic stretch (Figure S14 of the Supporting Information). When we compared the MSA study of p53 with the TANGO analysis for amyloid prediction, we found the presence of a highly conserved and highly amyloidogenic stretch of amino acids (p53 residues 250–257, PILTIITL) in the p53 DBD across most of the studied species (Figure 2). Moreover, we found another segment (YFTLQI) in the tetramerization domain of human p53 with relatively less amyloidogenic potential, which was less conserved among the studied species. The *in vitro* aggregation study using peptides corresponding to p53 (250–257) and p53 (327–332) showed that p53 (250–257) formed  $\beta$ -sheet rich structure at all the concentrations that were studied and formed amyloid fibrils revealed by electron microscopy (Figure 3A,B,H). ThT and CR dye binding studies confirmed the amyloid nature of these fibrils (Figure 3C–G). In contrast to p53 (250–257) however, p53 (327–332) (P6) did not show any conformational transition to  $\beta$ -sheet structure and did not demonstrate any fibril morphology after incubation for 15 days (Figure 4A,B,F). The peptides also did not show any other characteristics of amyloids such as CR and ThT binding even after incubation for 15 days (Figure 4C–E). The data suggest that irrespective of the aggregation tendency predicted by TANGO (although it was lower than that of P8), P6 did not form amyloid *in vitro*. The all atom MD simulation study suggested that p53 (250–257) not only has the ability to self-assemble into aggregated clusters at a very early time point during simulation but also displays a remarkable secondary structural transition from random coil to  $\beta$ -sheet rich structures, consistent with our *in vitro* data (Figure 5 and Figure S4 of the Supporting Information). Furthermore, the P8 peptides showed both parallel and antiparallel  $\beta$ -sheet tendencies during the MD simulation (Figure 5A). While the structural transition propensity of P8 is evident from our simulation, the exact orientation of peptides within these  $\beta$ -sheet rich structures cannot be ascertained from our simulation because of the limited time scale of the study. From the results of the simulation data, we can suggest that this ability of the p53 (250–257) stretch in the protein to acquire the  $\beta$ -sheet conformation could be crucial for the aggregation of native p53. Similar to that using p53 (250–257), the simulation study using p53 (327–332) from the p53 TD also showed significant self-assembly, however with negligible secondary structural

transition during the simulation (Figure 6 and Figure S8 of the Supporting Information). The simulation results thus reveal two vital differences in the self-association behavior of the two regions of p53: (i) a higher self-association potency of p53 (250–257) and (ii) higher structural transition ability of p53 (250–257) as opposed to p53 (327–332). Therefore, while p53 (250–257) progresses toward  $\beta$ -sheet rich aggregates, the region of the TD [p53 (327–332)] does not display any such structural predisposition. The data thus directly indicate that p53 (250–257) might be the most important region for p53 aggregation *in vitro* and in cells. Interestingly, upon analyzing the most frequently observed hydrogen bonds during the simulation, we found that residues Leu<sup>252</sup>, Ile<sup>254</sup>, Ile<sup>255</sup>, and Leu<sup>257</sup> play a crucial role in stabilizing the aggregates of p53 (250–257) (Table S16 of the Supporting Information). To further test these findings, we analyzed the aggregation profile of two chemically synthesized variants of the sequence PILTIITL [p53 (250–257)], PIRTIITR and PIRTRRTL, in which we substituted either Leu<sup>252</sup>, Ile<sup>254</sup>, Ile<sup>255</sup>, or Leu<sup>257</sup> with Arg, an amyloid gatekeeper amino acid residue (Figure 7A).<sup>32</sup> Our results suggest that the substitution of these three essential residues with Arg abrogates the amyloidogenic tendency of the otherwise strongly amyloidogenic segment PILTIITL (Figure 7B–E). These results thus validate the findings from our MD simulation. Similarly, the scrambled peptide, ITLPITLI, also did not show any amyloid aggregation *in vitro*, consistent with its TANGO analysis (Figure 7). This indicates that the amino acid sequence of the p53 (250–257) stretch, rather than its constituent residues, is responsible for its amyloidogenicity.

Amyloid formation is generally considered a “nucleation-dependent polymerization” process,<sup>48,78</sup> in which soluble native proteins are converted into “aggregation-templating nuclei”, which can drive the conversion of endogenous proteins into mature amyloid fibrils. Amyloid formation has also been shown to be accelerated by the addition of “preformed nuclei” (fibril seeds), which reduces the lag phase of nucleation.<sup>78</sup> Previously, many studies have reported that amyloids associated with several human diseases (such as Alzheimer’s and Parkinson’s) show infectious properties similar to those of prions (for a review, see ref 79), where preformed amyloids act as corruptive templates for the endogenous amplification of protein aggregation. This seeding mechanism is eventually responsible for the spreading and infectivity of the amyloid form of the protein. In fact, it has been demonstrated that p53 aggregates can be internalized into cells, which template the endogenous aggregation of functional p53, similar to other amyloid diseases.<sup>26,30</sup> Recently, it was hypothesized that p53 amyloid could also possess prion-like properties where preformed p53 aggregates can seed the aggregation of functional p53<sup>26,35,36</sup> and sequester other p53 paralogs such as p63 and p73.<sup>29</sup> This co-aggregation and templating effect of the preformed fibrils may contribute to the loss of function of native p53 as well as the gain-of-function effect of aggregated p53, leading to cancer progression and metastasis. Because the p53 (250–257) (P8) stretch formed amyloid *in vitro*, we asked whether the P8 fibrils could seed the aggregation of p53 *in vitro* and in cells. We chose the p53 core domain [p53 (94–312)] for our *in vitro* seeding study. The rationale for using the p53 core domain is that (i) the isolated p53 core is folded and functional and retains DNA binding activity<sup>68,69</sup> similar to full-length p53 and (ii) the p53 core has been widely used in many previous *in vitro* aggregation and amyloid formation studies.<sup>21,26,72</sup> Our data demonstrate that p53 alone did not show any aggregation, as measured by

ThT binding; however, in the presence of 1 and 2% P8 fibril seeds, p53 aggregation occurs substantially (Figure 8A). The seeded aggregates of the p53 core bind amyloid fibril-specific OC and oligomer-specific A11 antibodies, suggesting the presence of both fibrillar and prefibrillar oligomeric species (Figure 8C) among the p53 aggregates. Consistent with these data, previous *in vitro* studies have also shown that p53 aggregates contain both oligomers and fibrillar species.<sup>26</sup> Further, the P8 fibrils enter into cells when added exogenously and induce the aggregation of normal p53, as shown by the punctate nature of p53 inside the cells (Figure 8E,F). The results clearly indicate that P8 fibrils are also capable of seeding the aggregation of full-length p53 similar to the p53 core as demonstrated *in vitro*. Therefore, our data suggest that P8 fibril seeds can recognize its identical sequence in both the p53 core and the full-length protein and template their aggregation into large aggregates. These p53 aggregates might further interact with other proteins such as p63 and p73, as suggested previously,<sup>29</sup> causing an impairment of important cellular functions such as apoptosis. Additionally, p53 aggregates in cells might also sequester native, functional p53, thereby leading to a “dominant-negative” effect.<sup>80</sup>

Our experimental and simulation data thus suggest the presence of a putative amyloidogenic sequence in p53. In normal p53 (folded conformation), the aggregation-prone sequence may reside inside the core domain of the structure. However, if p53 mutations or various other factors expose this segment, this process may drive full-length p53 misfolding and aggregation, leading to its loss of function. Further studies are required to delineate the importance of this amyloidogenic region in driving the aggregation and amyloid formation by p53 *in vivo*. However, the knowledge of important contact residues that are responsible for p53 aggregation might aid in developing strategies for tackling aggregation-associated p53 loss of function in cancer progression.

## ASSOCIATED CONTENT

### Supporting Information

Additional data from the bioinformatic, MD simulation, and FTIR analysis of the aggregation stretches in p53. This material is available free of charge via the Internet at <http://pubs.acs.org>.

## AUTHOR INFORMATION

### Corresponding Author

\*Department of Biosciences and Bioengineering, IIT Bombay, Powai, Mumbai 400 076, India. E-mail: samirmaji@iitb.ac.in. Telephone: +(91-22) 2576-7774. Fax: +(91-22) 2572 3480.

### Author Contributions

S.K.M. designed the research. S.G., D.G., A.A., S.K.P., and N.N.J. conducted the *in vitro* experiments. S.R. performed *in silico* experiments. S.G., D.G., S.R., A.A., N.N.J., R.P., and S.K.M. analyzed and interpreted the data. S.G., S.R., and S.K.M. wrote the manuscript. S.G., D.G., and S.R. contributed equally to this work.

### Funding

The work was supported by Young Researcher Award Grant 2013 to S.K.M. from the Lady Tata Memorial Trust and an IITB-Healthcare Initiative Seed Grant to S.K.M.

### Notes

The authors declare no competing financial interest.

## ACKNOWLEDGMENTS

We acknowledge SAIF (IIT Bombay) for the electron microscopy facility. We also thank the IRCC central facility (IIT Bombay) for FTIR spectroscopy and confocal microscopy. We also acknowledge Dr. Shimul Salot for her input into the manuscript and Mrityunjoy Mondal for his help in conducting *in vitro* aggregation experiments with P8. D.G. acknowledges UGC (Government of India) for his fellowship.

## ABBREVIATIONS

BSA, bovine serum albumin; CD, circular dichroism; CR, Congo red; CTD, C-terminal domain; DBD, DNA binding domain; D-man, D-mannitol; EM, electron microscopy; FSD, Fourier self-deconvolution; MD, molecular dynamics; NTD, N-terminal domain; PBS, phosphate-buffered saline; PDB, Protein Data Bank; PMSF, phenylmethanesulfonyl fluoride; TD, tetramerization domain; TEM, transmission electron microscopy; ThT, thioflavin T.

## REFERENCES

- (1) Chiti, F., and Dobson, C. M. (2006) Protein misfolding, functional amyloid, and human disease. *Annu. Rev. Biochem.* 75, 333–366.
- (2) Maji, S. K., Wang, L., Greenwald, J., and Riek, R. (2009) Structure-activity relationship of amyloid fibrils. *FEBS Lett.* 583, 2610–2617.
- (3) Guijarro, J. I., Sunde, M., Jones, J. A., Campbell, I. D., and Dobson, C. M. (1998) Amyloid fibril formation by an SH3 domain. *Proc. Natl. Acad. Sci. U.S.A.* 95, 4224–4228.
- (4) Chiti, F., Webster, P., Taddei, N., Clark, A., Stefani, M., Ramponi, G., and Dobson, C. M. (1999) Designing conditions for *in vitro* formation of amyloid protofilaments and fibrils. *Proc. Natl. Acad. Sci. U.S.A.* 96, 3590–3594.
- (5) Dobson, C. M. (2001) The structural basis of protein folding and its links with human disease. *Philos. Trans. R. Soc., B* 356, 133–145.
- (6) Maji, S. K., Perrin, M. H., Sawaya, M. R., Jessberger, S., Vadodaria, K., Rissman, R. A., Singru, P. S., Nilsson, K. P., Simon, R., Schubert, D., Eisenberg, D., Rivier, J., Sawchenko, P., Vale, W., and Riek, R. (2009) Functional amyloids as natural storage of peptide hormones in pituitary secretory granules. *Science* 325, 328–332.
- (7) Fowler, D. M., Koulov, A. V., Alory-Jost, C., Marks, M. S., Balch, W. E., and Kelly, J. W. (2006) Functional amyloid formation within mammalian tissue. *PLoS Biol.* 4, e6.
- (8) Fowler, D. M., Koulov, A. V., Balch, W. E., and Kelly, J. W. (2007) Functional amyloid: From bacteria to humans. *Trends Biochem. Sci.* 32, 217–224.
- (9) Levine, A. J. (1997) p53, the cellular gatekeeper for growth and division. *Cell* 88, 323–331.
- (10) Harris, S. L., and Levine, A. J. (2005) The p53 pathway: Positive and negative feedback loops. *Oncogene* 24, 2899–2908.
- (11) Vousden, K. H., and Lu, X. (2002) Live or let die: The cell's response to p53. *Nat. Rev. Cancer* 2, 594–604.
- (12) Oren, M., Maltzman, W., and Levine, A. J. (1981) Post-translational regulation of the 54K cellular tumor antigen in normal and transformed cells. *Mol. Cell. Biol.* 1, 101–110.
- (13) Slade, N., and Moll, U. M. (2003) Mutational analysis of p53 in human tumors: Immunocytochemistry. *Methods Mol. Biol.* 234, 231–243.
- (14) Muller, P. A. J., and Vousden, K. H. (2014) Mutant p53 in Cancer: New Functions and Therapeutic Opportunities. *Cancer Cell* 25, 304–317.
- (15) Dong, P., Karaayvaz, M., Jia, N., Kaneuchi, M., Hamada, J., Watari, H., Sudo, S., Ju, J., and Sakuragi, N. (2013) Mutant p53 gain-of-function induces epithelial-mesenchymal transition through modulation of the miR-130b-ZEB1 axis. *Oncogene* 32, 3286–3295.

- (16) Moll, U. M., LaQuaglia, M., Benard, J., and Riou, G. (1995) Wild-type p53 protein undergoes cytoplasmic sequestration in undifferentiated neuroblastomas but not in differentiated tumors. *Proc. Natl. Acad. Sci. U.S.A.* 92, 4407–4411.
- (17) Moll, U. M., Ostermeyer, A. G., Haladay, R., Winkfield, B., Frazier, M., and Zambetti, G. (1996) Cytoplasmic sequestration of wild-type p53 protein impairs the G1 checkpoint after DNA damage. *Mol. Cell. Biol.* 16, 1126–1137.
- (18) Moll, U. M., Riou, G., and Levine, A. J. (1992) Two distinct mechanisms alter p53 in breast cancer: Mutation and nuclear exclusion. *Proc. Natl. Acad. Sci. U.S.A.* 89, 7262–7266.
- (19) Bosari, S., Viale, G., Bossi, P., Maggioni, M., Coggi, G., Murray, J. J., and Lee, A. K. (1994) Cytoplasmic accumulation of p53 protein: An independent prognostic indicator in colorectal adenocarcinomas. *J. Natl. Cancer Inst.* 86, 681–687.
- (20) Bosari, S., Viale, G., Roncalli, M., Graziani, D., Borsani, G., Lee, A. K., and Coggi, G. (1995) p53 gene mutations, p53 protein accumulation and compartmentalization in colorectal adenocarcinoma. *Am. J. Pathol.* 147, 790–798.
- (21) Ishimaru, D., Andrade, L. R., Teixeira, L. S., Quesado, P. A., Maiolino, L. M., Lopez, P. M., Cordeiro, Y., Costa, L. T., Heckl, W. M., Weissmuller, G., Foguel, D., and Silva, J. L. (2003) Fibrillar aggregates of the tumor suppressor p53 core domain. *Biochemistry* 42, 9022–9027.
- (22) Lee, A. S., Galea, C., DiGiammarino, E. L., Jun, B., Murti, G., Ribeiro, R. C., Zambetti, G., Schultz, C. P., and Kriwacki, R. W. (2003) Reversible amyloid formation by the p53 tetramerization domain and a cancer-associated mutant. *J. Mol. Biol.* 327, 699–709.
- (23) Rigacci, S., Bucciantini, M., Relini, A., Pesce, A., Gliozzi, A., Berti, A., and Stefani, M. (2008) The (1–63) region of the p53 transactivation domain aggregates in vitro into cytotoxic amyloid assemblies. *Biophys. J.* 94, 363S–364S.
- (24) Butler, J. S., and Loh, S. N. (2003) Structure, function, and aggregation of the zinc-free form of the p53 DNA binding domain. *Biochemistry* 42, 2396–2403.
- (25) Lasagna-Reeves, C. A., Clos, A. L., Castillo-Carranza, D., Sengupta, U., Guerrero-Munoz, M., Kelly, B., Wagner, R., and Kayed, R. (2013) Dual role of p53 amyloid formation in cancer; loss of function and gain of toxicity. *Biochem. Biophys. Res. Commun.* 430, 963–968.
- (26) Ano Bom, A. P., Rangel, L. P., Costa, D. C., de Oliveira, G. A., Sanches, D., Braga, C. A., Gava, L. M., Ramos, C. H., Cepeda, A. O., Stumbo, A. C., De Moura Gallo, C. V., Cordeiro, Y., and Silva, J. L. (2012) Mutant p53 aggregates into prion-like amyloid oligomers and fibrils: Implications for cancer. *J. Biol. Chem.* 287, 28152–28162.
- (27) Levy, C. B., Stumbo, A. C., Ano Bom, A. P., Portari, E. A., Cordeiro, Y., Silva, J. L., and De Moura-Gallo, C. V. (2011) Co-localization of mutant p53 and amyloid-like protein aggregates in breast tumors. *Int. J. Biochem. Cell Biol.* 43, 60–64.
- (28) Nieva, J., Song, B. D., Rogel, J. K., Kujawara, D., Altobel, L., III, Izharrudin, A., Boldt, G. E., Grover, R. K., Wentworth, A. D., and Wentworth, P., Jr. (2011) Cholesterol secosterol aldehydes induce amyloidogenesis and dysfunction of wild-type tumor protein p53. *Chem. Biol.* 18, 920–927.
- (29) Xu, J., Reumers, J., Couceiro, J. R., De Smet, F., Gallardo, R., Rudyak, S., Cornelis, A., Rozenski, J., Zwolinska, A., Marine, J.-C., Lambrechts, D., Suh, Y.-A., Rousseau, F., and Schymkowitz, J. (2011) Gain of function of mutant p53 by coaggregation with multiple tumor suppressors. *Nat. Chem. Biol.* 7, 285–295.
- (30) Forget, K. J., Tremblay, G., and Roucou, X. (2013) p53 Aggregates Penetrate Cells and Induce the Co-Aggregation of Intracellular p53. *PLoS One* 8, e69242.
- (31) Fernandez-Escamilla, A., Rousseau, F., Schymkowitz, J., and Serrano, L. (2004) Prediction of sequence-dependent and mutational effects on the aggregation of peptides and proteins. *Nat. Biotechnol.* 22, 1302–1306.
- (32) Reumers, J., Maurer-Stroh, S., Schymkowitz, J., and Rousseau, F. (2009) Protein sequences encode safeguards against aggregation. *Hum. Mutat.* 30, 431–437.
- (33) Maurer-Stroh, S., Debulpaepe, M., Kuemmerer, N., de la Paz, M. L., Martins, I. C., Reumers, J., Morris, K. L., Copland, A., Serpell, L., Serrano, L., Schymkowitz, J. W., and Rousseau, F. (2010) Exploring the sequence determinants of amyloid structure using position-specific scoring matrices. *Nat. Methods* 7, 237–242.
- (34) Conchillo-Sole, O., de Groot, N., Aviles, F., Vendrell, J., Daura, X., and Ventura, S. (2007) AGGRESCAN: A server for the prediction and evaluation of “hot spots” of aggregation in polypeptides. *BMC Bioinf.* 8, 65.
- (35) Rangel, L. P., Costa, D. C. F., Vieira, T. C. R. G., and Silva, J. L. (2014) The aggregation of mutant p53 produces prion-like properties in cancer. *Prion* 8, 75–84.
- (36) Silva, J. L., Gallo, C. V. D. M., Costa, D. C. F., and Rangel, L. P. (2014) Prion-like aggregation of mutant p53 in cancer. *Trends Biochem. Sci.* 39, 260–267.
- (37) Trovato, A., Seno, F., and Tosatto, S. C. E. (2007) The PASTA server for protein aggregation prediction. *Protein Eng., Des. Sel.* 20, 521–523.
- (38) Thompson, M., Sievers, S., Karanicolas, J., Ivanova, M., Baker, D., and Eisenberg, D. (2006) The 3D profile method for identifying fibril-forming segments of proteins. *Proc. Natl. Acad. Sci. U.S.A.* 103, 4074–4078.
- (39) Sievers, F., Wilm, A., Dineen, D., Gibson, T. J., Karplus, K., Li, W., Lopez, R., McWilliam, H., Remmert, M., Soding, J., Thompson, J. D., and Higgins, D. G. (2011) Fast, scalable generation of high-quality protein multiple sequence alignments using Clustal Omega. *Mol. Syst. Biol.* 7, 539.
- (40) Baudot, A., Martin, D., Mouren, P., Chevenet, F., Guenoche, A., Jacq, B., and Brun, C. (2006) PRODISTIN web site: A tool for the functional classification of proteins from interaction networks. *Bioinformatics* 22, 248–250.
- (41) Ayed, A., Mulder, F. A. A., Yi, G.-S., Lu, Y., Kay, L. E., and Arrowsmith, C. H. (2001) Latent and active p53 are identical in conformation. *Nat. Struct. Mol. Biol.* 8, 756–760.
- (42) Jha, N. N., Anoop, A., Ranganathan, S., Mohite, G. M., Padinhateeri, R., and Maji, S. K. (2013) Characterization of Amyloid Formation by Glucagon-Like Peptides: Role of Basic Residues in Heparin-Mediated Aggregation. *Biochemistry* 52, 8800–8810.
- (43) Anoop, A., Ranganathan, S., Dhaked, B. D., Jha, N. N., Pratihar, S., Ghosh, S., Sahay, S., Kumar, S., Das, S., Komrabail, M., Agarwal, K., Jacob, R. S., Singru, P., Bhaumik, P., Padinhateeri, R., Kumar, A., and Maji, S. K. (2014) Elucidating the role of disulfide bond on amyloid formation and fibril reversibility of somatostatin-14: Relevance to its storage and secretion. *J. Biol. Chem.* 289, 16884–16903.
- (44) LeVine, H., III (1999) Quantification of β-sheet amyloid fibril structures with thioflavin T. *Methods Enzymol.* 309, 274–284.
- (45) Klunk, W. E., Jacob, R. F., and Mason, R. P. (1999) Quantifying amyloid by Congo red spectral shift assay. *Methods Enzymol.* 309, 285–305.
- (46) Westerman, G. T., Johnson, K. H., and Westerman, P. (1999) Staining methods for identification of amyloid in tissue. *Methods Enzymol.* 309, 3–25.
- (47) Maji, S. K., Schubert, D., Rivier, C., Lee, S., Rivier, J. E., and Riek, R. (2008) Amyloid as a depot for the formulation of long-acting drugs. *PLoS Biol.* 6, e17.
- (48) Jarrett, J. T., and Lansbury, P. T., Jr. (1993) Seeding “one-dimensional crystallization” of amyloid: A pathogenic mechanism in Alzheimer’s disease and scrapie? *Cell* 73, 1055–1058.
- (49) Barth, A. (2007) Infrared spectroscopy of proteins. *Biochim. Biophys. Acta* 1767, 1073–1101.
- (50) Jackson, M., and Mantsch, H. H. (1995) The use and misuse of FTIR spectroscopy in the determination of protein structure. *Crit. Rev. Biochem. Mol. Biol.* 30, 95–120.
- (51) Ghosh, D., Dutta, P., Chakraborty, C., Singh, P. K., Anoop, A., Jha, N. N., Jacob, R. S., Mondal, M., Mankar, S., Das, S., Malik, S., and Maji, S. K. (2014) Complexation of Amyloid Fibrils with Charged Conjugated Polymers. *Langmuir* 30, 3775–3786.

- (52) Ghosh, D., Mondal, M., Mohite, G. M., Singh, P. K., Ranjan, P., Anoop, A., Ghosh, S., Jha, N. N., Kumar, A., and Maji, S. K. (2013) The Parkinson's Disease-Associated H50Q Mutation Accelerates  $\alpha$ -Synuclein Aggregation *in vitro*. *Biochemistry* 52, 6925–6927.
- (53) Klimov, D. K., and Thirumalai, D. (2003) Dissecting the assembly of  $\text{A}\beta(16–22)$  amyloid peptides into antiparallel  $\beta$ -sheets. *Structure* 11, 295–307.
- (54) Urbanc, B., Cruz, L., Teplow, D. B., and Stanley, H. E. (2006) Computer simulations of Alzheimer's amyloid  $\beta$  protein folding and assembly. *Curr. Alzheimer Res.* 3, 493–504.
- (55) Ma, B., and Nussinov, R. (2006) Simulations as analytical tools to understand protein aggregation and predict amyloid conformation. *Curr. Opin. Chem. Biol.* 10, 445–452.
- (56) Ranganathan, S., Singh, P. K., Singh, U., Singru, P. S., Padinhateeri, R., and Maji, S. K. (2012) Molecular Interpretation of ACTH- $\beta$ -Endorphin Coaggregation: Relevance to Secretory Granule Biogenesis. *PLoS One* 7, e31924.
- (57) Phillips, J. C., Braun, R., Wang, W., Gumbart, J., Tajkhorshid, E., Villa, E., Chipot, C., Skeel, R. D., Kale, L., and Schulten, K. (2005) Scalable molecular dynamics with NAMD. *J. Comput. Chem.* 26, 1781–1802.
- (58) Humphrey, W., Dalke, A., and Schulten, K. (1996) VMD: Visual molecular dynamics. *J. Mol. Graphics* 14, 27–38.
- (59) Kayed, R., Head, E., Sarsoga, F., Saing, T., Cotman, C., Necula, M., Margol, L., Wu, J., Breydo, L., Thompson, J., Rasool, S., Gurlo, T., Butler, P., and Glabe, C. (2007) Fibril specific, conformation dependent antibodies recognize a generic epitope common to amyloid fibrils and fibrillar oligomers that is absent in prefibrillar oligomers. *Mol. Neurodegener.* 2, 18.
- (60) Kayed, R., Head, E., Thompson, J. L., McIntire, T. M., Milton, S. C., Cotman, C. W., and Glabe, C. G. (2003) Common structure of soluble amyloid oligomers implies common mechanism of pathogenesis. *Science* 300, 486–489.
- (61) Cui, H., Schroering, A., and Ding, H.-F. (2002) p53 Mediates DNA Damaging Drug-induced Apoptosis through a Caspase-9-dependent Pathway in SH-SY5Y Neuroblastoma Cells. *Mol. Cancer Ther.* 1, 679–686.
- (62) Joerger, A. C., and Fersht, A. R. (2008) Structural Biology of the Tumor Suppressor p53. *Annu. Rev. Biochem.* 77, 557–582.
- (63) Ollmann, M., Young, L. M., Di Como, C. J., Karim, F., Belvin, M., Robertson, S., Whittaker, K., Demsky, M., Fisher, W. W., Buchman, A., Duyk, G., Friedman, L., Prives, C., and Kopczynski, C. (2000) *Drosophila* p53 is a structural and functional homolog of the tumor suppressor p53. *Cell* 101, 91–101.
- (64) Schumacher, B., Hofmann, K., Boulton, S., and Gartner, A. (2001) The *C. elegans* homolog of the p53 tumor suppressor is required for DNA damage-induced apoptosis. *Curr. Biol.* 11, 1722–1727.
- (65) van der Wilk, F., Dullemans, A. M., Verbeek, M., and van den Heuvel, J. F. (1999) Isolation and characterization of APSE-1, a bacteriophage infecting the secondary endosymbiont of *Acyrthosiphon pisum*. *Virology* 262, 104–113.
- (66) Greenfield, N. J. (2007) Analysis of the kinetics of folding of proteins and peptides using circular dichroism. *Nat. Protoc.* 1, 2891–2899.
- (67) Hiramatsu, H., and Kitagawa, T. (2005) FT-IR approaches on amyloid fibril structure. *Biochim. Biophys. Acta* 1753, 100–107.
- (68) Selivanova, G., Ryabchenko, L., Jansson, E., Iotsova, V., and Wiman, K. G. (1999) Reactivation of Mutant p53 through Interaction of a C-Terminal Peptide with the Core Domain. *Mol. Cell. Biol.* 19, 3395–3402.
- (69) Bullock, A. N., Henckel, J., and Fersht, A. R. (2000) Quantitative analysis of residual folding and DNA binding in mutant p53 core domain: Definition of mutant states for rescue in cancer therapy. *Oncogene* 19, 1245–1256.
- (70) Olivier, M., Eeles, R., Hollstein, M., Khan, M. A., Harris, C. C., and Hainaut, P. (2002) The IARC TP53 database: New online mutation analysis and recommendations to users. *Hum. Mutat.* 19, 607–614.
- (71) Freed-Pastor, W. A., and Prives, C. (2012) Mutant p53: One name, many proteins. *Genes Dev.* 26, 1268–1286.
- (72) Bullock, A. N., Henckel, J., DeDecker, B. S., Johnson, C. M., Nikolova, P. V., Proctor, M. R., Lane, D. P., and Fersht, A. R. (1997) Thermodynamic stability of wild-type and mutant p53 core domain. *Proc. Natl. Acad. Sci. U.S.A.* 94, 14338–14342.
- (73) Ang, H. C., Joerger, A. C., Mayer, S., and Fersht, A. R. (2006) Effects of Common Cancer Mutations on Stability and DNA Binding of Full-length p53 Compared with Isolated Core Domains. *J. Biol. Chem.* 281, 21934–21941.
- (74) Ostermeyer, A. G., Runko, E., Winkfield, B., Ahn, B., and Moll, U. M. (1996) Cytoplasmically sequestered wild-type p53 protein in neuroblastoma is relocated to the nucleus by a C-terminal peptide. *Proc. Natl. Acad. Sci. U.S.A.* 93, 15190–15194.
- (75) Giannakakou, P., Sackett, D. L., Ward, Y., Webster, K. R., Blagosklonny, M. V., and Fojo, T. (2000) p53 is associated with cellular microtubules and is transported to the nucleus by dynein. *Nat. Cell Biol.* 2, 709–717.
- (76) Shaulsky, G., Goldfinger, N., Tosky, M. S., Levine, A. J., and Rotter, V. (1991) Nuclear localization is essential for the activity of p53 protein. *Oncogene* 6, 2055–2065.
- (77) Muller, P. A. J., and Vousden, K. H. (2013) p53 mutations in cancer. *Nat. Cell Biol.* 15, 2–8.
- (78) Harper, J. D., and Lansbury, P. T., Jr. (1997) Models of amyloid seeding in Alzheimer's disease and scrapie: Mechanistic truths and physiological consequences of the time-dependent solubility of amyloid proteins. *Annu. Rev. Biochem.* 66, 385–407.
- (79) Jucker, M., and Walker, L. C. (2013) Self-propagation of pathogenic protein aggregates in neurodegenerative diseases. *Nature* 501, 45–51.
- (80) Silva, J. L., Vieira, T. C., Gomes, M. P., Bom, A. P., Lima, L. M., Freitas, M. S., Ishimaru, D., Cordeiro, Y., and Foguel, D. (2010) Ligand binding and hydration in protein misfolding: Insights from studies of prion and p53 tumor suppressor proteins. *Acc. Chem. Res.* 43, 271–279.